Analysis of the Fluorescence Transient

Reto J. Strasser
Bioenergetics Laboratory, University of Geneva
CH-1254 Jussy/Geneva, Switzerland
Tel.: ++ 41 22 759 9940, Fax: ++ 41 22 759 9945, e-mail: Reto.Strasser@bioen.unige.ch
http://www.unige.ch/sciences/biologie/bioen/
http://come.to./bionrj

Merope Tsimilli- Michael
Ministry of Education and Culture, Nicosia CY-1434, Cyprus
Tel.: ++ 357 9456625, e-mail: tsimicha@spidernet.com.cy

Alaka Srivastava
Brown University, Biology Department, Providence, RI 02912, USA
Tel.: ++ 1 4018633075, e-mail: Alaka Srivastava@brown.edu

TABLE OF CONTENTS

Summary

I. Introduction

II. The Theoretical Background

A. The theory of Energy Fluxes in Biomembranes: The Basics

B. Energy Fluxes in the Photosynthetic Unit

(a) at the extremes

(b) at any intermediate redox state between the extremes

C. From Biophysical to Experimental Parameters

1. The fluorescence signals

(a) at the extremes

(b) at any intermediate redox state between the extremes

2. Experimental vs. theoretical resolution

3. Yields and probabilities

4. The quantum yield for primary photochemistry

III. Fluorescence Transients in the Presence of Diuron at Room Temperature

A. The Area above the Fluorescence Transient

B. The Shape of the Fluorescence Transient

C. Determination of the Over-All Grouping Probability

IV. Fluorescence Transients at Low Temperature

A. The Fluorescence Transient at 695 nm

B. Correlation of Fluorescence Transients at 685 nm, 695 nm and 735 nm

V. Polyphasic Fluorescence Transients in Vivo

A. Simultaneous Kautsky transients at two wavelengths

B. The JIP-test as a tool for fast in vivo vitality screenings

1. Fluxes and yields

2. Non-Q_A-reducing reaction centers - Silent reaction centers functioning as heat sinks

3. Performance indexes and driving forces

4. The complementary area and the turnover number

5. The time t_{F_M} to reach F_M and the average fraction of open reaction centers

6. Determination of the over-all grouping probability

7. Non-Q_B-reducing reaction centers

8. Summarizing the JIP-test

C. The K-Step: A probe of the PSII donor side

D. Numerical Simulations of the Polyphasic Fluorescence Rise

E. E. Simultaneous measurements of fluorescence transients and P700 oxidation

VI. Concluding Remarks

VII. References

Summary

This chapter deals with direct chlorophyll (Chl) *a* fluorescence signals and describes how fluorescence transients exhibited by photosynthetic organisms under different conditions can be analyzed to provide information about the structure, conformation and function of the photosynthetic apparatus and especially of photosystem (PS) II. The analytical formulation of the biophysics of the photosynthetic apparatus, according to models of different complexity regarding both the architecture of the photosynthetic unit and the modes of energetic communication among the pigment assemblies, as well as their links to the experimental fluorescence signals are derived, based on the Theory of Energy Fluxes in Biomembranes. Starting with fluorescence transients exhibited (a) in the presence of DCMU and (b) at low temperature (77K), i.e. under conditions that reduce the complexity of the in vivo system, the chapter then focuses on the analysis of the polyphasic fluorescence transient under physiological conditions. The analysis of the fluorescence rise O-J-I-P by the JIP-test, which can be applied at any physiological state and for the study of any state transition, is presented in detail with the full derivation of the formulae for the constellation of experimentally accessible parameters, among which the specific and phenomenological energy fluxes, the yields, the fraction of reactions centers that can not reduce the primary quinone acceptor $\mathbf{Q_A}$ (heat sinks or "silent" centers) or the secondary quinone acceptor $\mathbf{Q_B}$, as well as the overall grouping probability. The influence of the donor side on the fluorescence yield, with emphasis on the appearance under certain conditions of an early step (K-step, at about 200 μs) in the regular O-J-I-P transient, related with the inactivation of the water splitting system, is also discussed. Moreover, results from numerical simulations of the O-J-I-P transient are summarized with emphasis on the investigation of the possible role of the primary acceptor pheophytin (**Pheo**). The chapter closes with the presentation of very recent advancements, achieved by simultaneous in vivo measurements (both with μs time resolution) of fluorescence transients and P700 oxidation.

Abbreviations

B fraction of closed reaction centers
Chl chlorophyll
DCMU 3-(3,4-dichlorophenyl)-1,1-dimethylurea
CS excited cross section
LHC light harvesting complex *a/b*
Pheo (or Ph) pheophytin
PS photosystem
Q_A primary quinone acceptor of PSII
Q_B secondary quinone acceptor of PSII
OEC oxygen evolving complex
RC reaction center.

I. Introduction

Many experimental techniques are today available for the investigation of the energetic behavior of a photosynthetic system. Chl *a* fluorescence, though corresponding to a very small fraction of the dissipated energy from the photosynthetic apparatus, is widely accepted to provide an access to the understanding of its structure and function. There is a general agreement that at room temperature Chl *a* fluorescence of plants in the spectral region 680-740 nm is almost exclusively emitted by PSII and it can therefore serve as an intrinsic probe of the fate of its excitation energy (for reviews see Papageorgiou 1975; Briantais et al. 1986; Krause and Weiss 1991; Dau 1994; Govindjee 1995; Lazár 1999). Both the spectra and the kinetics of Chl *a* fluorescence have been proven to be powerful, non-invasive tools for such investigations.

Concerning the kinetics, the fluorimeters used are of two basic types, recording fluorescence signals induced by continuous or modulated excitation. A lot of debates have been published, comparing the two techniques and favoring the one or the other. However, as they both measure the fluorescence signal emitted by the photosynthetic machinery, the provided information cannot be contradictory. What is really important is to make the links between the fluorescence signal and the biophysics of the system, for which an appropriate theory/methodology is needed.

In this chapter, the derivation of the links between the biophysics of the photosynthetic apparatus and the fluorescence signals and their analytical formulations is based on the Theory of Energy Fluxes in Biomembranes (Strasser 1978, 1981) and the basic concept that the fluorescence yield of PSII is determined by the state - open or closed - of the reaction center (RC), while in section V.B.2 the role of "silent RCs" will also be discussed. Without further assumptions, models of different complexity concerning energetic communication will be presented and the energy flux theory, summarized in section II.A, will be applied for the derivation of analytical solutions for the energy influxes in open and closed RCs (section II.B). The correlation of phenomenological with biophysical parameters will be discussed in section II.C, taking into account that the resolution of fluorescence signals is lower than theoretical resolutions.

For the analysis of the fluorescence transients the dogma that the state of the PSII RCs is defined by the redox state of the primary quinone acceptor $\mathbf{Q_A}$, based on the quencher theory of Duysens and Sweers (1963) and adopted by the majority of researchers, will be accepted as a first approach, while in section V.D evidences for the possible role of the primary acceptor Pheo will be presented.

This chapter deals only with direct fluorescence signals and the analysis of transients under different conditions, presented in a sequence following the chronological order of their investigation and utilization. Sixty years after the report of the original Kautsky transient (Kautsky and Hirsch 1931) the same transient O-P-S was recorded with a high time-resolution and, plotted on a logarithmic time basis (Fig. 1), revealed a shape with many phases, rich in information for the status of the system in vivo (Strasser and Govindjee 1992a, 1992b).

In the time between, the utilization of DCMU to inhibit the electron flow at the PSII acceptor side and of low temperature (77 K) to block the electron flow both at the donor and the acceptor side of PSII facilitated the investigations, as both treatments reduce the complexity of the *in vivo* system and permitted the study of simpler components. Though the latter was also a disadvantage, the studies in the presence of DCMU (section III) and at low temperature (section IV) were very important for the advancement of the knowledge and understanding of the biophysics of the photosynthetic machinery. Low temperature permits also the correlation of the fluorescence transients exhibited by the PSII core antenna, PSII light harvesting complex *a/b* (LHC) and PSI, providing adequate information about energy exchange within PSII and energy distribution between the two photosystems.

Section V deals with the analysis of the fluorescence transients in vivo. Simultaneously recorded transients at two wavelengths, 685 and 715 nm, are utilized by the method described in section V.A to provide information about the state 1 to state 2 transition reflected in the P-S decline of a Kautsky

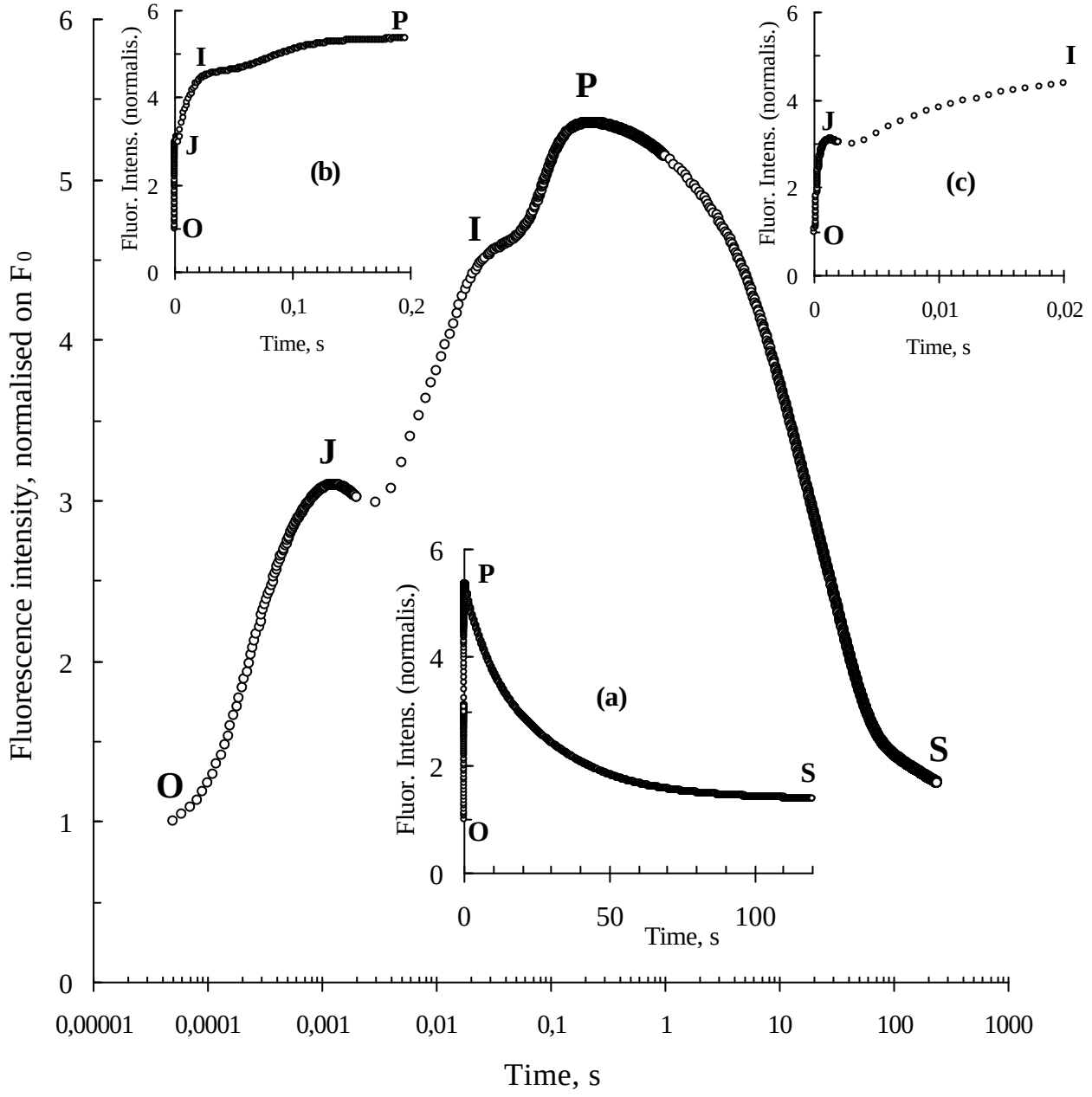

Fig. 1. A typical Kautsky fluorescence transient exhibited upon illumination of a dark-adapted photosynthetic sample by saturating light (red light of 600 Wm^{-2}) and plotted on a logarithmic time scale. Inserts show the same transient on different linear time scales: (a) up to 120 s, (b) up to 200 ms and (c) up to 20 ms. For details see text.

transient. The analysis of the fluorescence rise O-J-I-P by the JIP-test, which can be applied at any physiological state and for the study of any state transition, is presented in detail. The derivation of formulae for the translation of selected data stored in O-J-I-P transient to structural and functional parameters quantifying PSII behavior is analytically described. The calculated parameters are: the specific (per RC) and phenomenological (per excited cross section, CS) energy fluxes for absorption, trapping and electron transport; the quantum yields for primary photochemistry and for electron transport, as well as the efficiency by which a trapped exciton moves an electron into the electron transport chain further than $\mathbf{Q_A^-}$; the density of the RCs which, by comparison of samples under different conditions, leads to the calculation of the difference in the fraction of non-Q_A reducing RCs (heat sinks or "silent" centers); performance indexes and driving forces; the turnover number for $\mathbf{Q_A}$ reduction until all $\mathbf{Q_A}$ are reduced; the average redox state of $\mathbf{Q_A}$ in the time span from 0 until the maximum fluorescence is achieved; the over-all grouping probability. The fraction of non-Q_B reducing RCs is also estimated by double hit experiments.

The influence of the donor side on the fluorescence yield, with emphasis on the appearance under certain conditions of an early step (K-step, at about 200 μs) in the regular O-J-I-P transient, related with the inactivation of the water splitting system, is discussed in section V.C, while section V.D refers to numerical simulations of the O-J-I-P transient, focusing on the possible role of the primary acceptor pheophytin. Very recent advancements referring to simultaneous in vivo measurements of fluorescence transients and P700 oxidation with the same time resolution (μs range) are included in the chapter (section V.E), as well as an outline of future perspectives (section V.F).

II. The Theoretical Background

A. The theory of Energy Fluxes in Biomembranes: The Basics

An energetic concept and a general applicable theory/methodology is needed to describe any proposed model. Thereafter, the behavior of the system according to the model can be predicted and the predictions can be compared with the experimentally measured functions of the photosynthetic system.

In our approach, the derivation of the links between the energetic behavior of the photosynthetic apparatus and the fluorescence signals is based on the Theory of Energy Fluxes in Biomembranes (Strasser 1978, 1981), which addresses to any pigment assemblies in any type of biomembrane. The theory has been mainly applied for studies of photosynthetic units in higher plants and algae. It has also been used for the formulation of the behavior of PSI and PSII in cyanobacteria (Karapetyan et al. 1999), of isolated pigment complexes, e.g. the LHC (Gruszecki et al. 1994), of the protochlorophyllide to chlorophyllide photoreduction (Sironval et al. 1981, 1984; Strasser 1984) and it can be furthermore applied for any type of energy exchange among any biochromophore, as for example flavoproteins or bacteriorhodopsin (Strasser 1980; Strasser and Butler 1980).

The methodological frame of the energy flux theory permits the rigorous definition of all terms often used in the analysis of energy distribution in the photosynthetic apparatus (flux, yield, probability and rate constants of energy transfer). The theory introduces and defines five basic and distinct magnitudes related to any pigment system **i** (see Table 1) and postulates that, for any possible complex arrangement of interconnected pigment systems, their energetic communication can be expressed by simple equations, easily solved analytically, in terms of the basic magnitudes, as shown in Table 1.

It is worth pointing out that (a) as influxes and outfluxes are rapidly equilibrated in a pigment system **i**, the total outflux is equal to the total influx; (b) it is assumed that each individual de-excitation from **i** to **j** is of first order (in case of second order de-excitations, the de-excitation flux would be expressed by the product of the exciton density, the rate constant and the concentration of the energy acceptor).

Table 1. The five basic magnitudes referring to a pigment system **i**, as defined in the Theory of Energy Fluxes in Biomembranes

ENERGY FLUXES		
Energy Influxes to pigment system **i** or **excitation rates** of **i**	J_i	– light absorption flux by pigment system **i**
	E_{hi}	– energy transfer flux from a pigment system **h** to pigment system **i**
$E_i = J_i + \sum_h E_{hi}$ (eq.1)	E_i	– total energy influx to pigment system **i** (or total excitation rate of **i**)
Energy Outfluxes from pigment system **i** or **de-excitation rates** of **i** as transfers/transductions to any location/form **j** (**j** being **m**, **t**, **D**)	E_{im}	– energy transfer flux from pigment system **i** to a pigment system **m**
	E_{it}	– energy outflux from pigment system **i** that is transformed (e.g. for charge separation)
	E_{iD}	– energy dissipation flux as ▪ heat dissipation flux E_{iH} ▪ fluorescence flux E_{iF} (experimentally measured as F_i)
$E_i = \sum_j E_{ij}$ (eq.2)	E_i	– total energy outflux from **i** (or total de-excitation rate of **i**), equal to the total energy influx to **i**
RATE CONSTANTS	k_{ij}	– rate constant for the energy flux from **i** to **j**
LIFETIME $t_i = 1 / \sum_j k_{ij}$ (eq.3)	t_i	– lifetime of the excited state of pigment system **i**
PROBABILITIES $p_{ij} = E_{ij} / \sum_j E_{ij} = E_{ij} / E_i$ (eq. 4) $p_{ij} = k_{ij} / \sum_j k_{ij} = k_{ij} \cdot t_i$ (eq. 5)	p_{ij}	– probability that an exciton is transferred/ transduced from pigment system **i** to a location/form **j**
EXCITON DENSITY $P_i^* = E_i \cdot t_i$ (eq. 6)	P_i^*	– concentration of excited pigments **i** or energy content of the excited pigment system **i**

From the equations presented in Table 1 it is deduced that all types of de-excitation fluxes from a pigment system **i** to any destination **j** can be equivalently expressed as:

$$E_{ij} = E_i \cdot p_{ij} = E_i \cdot (t_i \cdot k_{ij}) = (E_i \cdot t_i) \cdot k_{ij} = P_i^* \cdot k_{ij} \qquad \text{(eq. 7)}$$

B. Energy Fluxes in the Photosynthetic Unit

With the energy flux theory any model, assuming any structure (chemical inventory and architecture of pigment assemblies) in the photosynthetic apparatus and any conformation (rate constants) regarding energetic communication, can easily be formulated mathematically, leading to the derivation of analytical equations for the constellation of energy fluxes defining the function of the system (Strasser 1978, 1981). However, since the goal is to apply the energy flux theory for the interpretation and utilization of the phenomenological observations – here of the fluorescence of a photosynthetic system –, the complexity of a model is meaningful if the experimental signal has the according resolution.

The models schematically presented in Fig. 2 use boxes – squares for pigment pools and round for RC – to present structure, and arrows to present energy fluxes E_{ij} and, hence, to demonstrate indirectly (eq. 7) the conformation, i.e. the rate constants k_{ij}. All of them are identical concerning structure, the complexity of which is reduced from the many pigment assemblies to three (tripartite model, see e.g. Butler and Strasser 1977a; Strasser 1986), in accordance with the limitation of fluorescence measurements in revealing further heterogeneity. These tripartite models assume two pigment systems in PSII, namely the distal antenna or LHC (labeled as **3**) and the proximal or core antenna assembly (labeled as **2**), channeling finally excitation energy to the PSII reaction center (labeled as **b**), while the PSI pigment systems channeling excitation energy to the PSI reaction center (labeled as **a**) are regarded as one site (labeled as **1**). Note that, for simplicity of the scheme, PSI is not shown as structure but only indirectly by the arrows corresponding to the energy migration fluxes.

In principal, the excited PSII pigment pools (**2** and **3**) can perform, except for primary photochemistry, all types of de-excitation with probabilities governed by their conformation, while an excited RC, depending on its conformation, can perform a single but any type of de-excitation, including energy conservation in primary photochemistry $PA \rightarrow P^+A^-$ (**P** standing for P680, i.e. the RC, and **A** for the primary electron acceptor). Models 1 and 2 are statistical models, in the sense that they pool together units with RCs of different conformation.

Model 1 keeps the full complexity, assuming light absorption as well as energy dissipation (with E_{iD} standing for total dissipation, i.e. heat and fluorescence, $E_{iD} = E_{iH} + E_{iF}$) by all PSII sites, variable energetic communication between core antenna and RC within a PSII unit (trapping term **T**), between core antenna and LHC within a PSII unit (coupling term **C**), between same sites (RC-RC, core antenna – core antenna and LHC – LHC) of neighbor PSII units (grouping **G**, a term introduced by Strasser (1978, 1981) for variable connectivity, i.e. with probability from zero to unity) and between PSII and PSI sites (migration **M**). The terms trapping product $T = p_{2b}p_{b2}$ and coupling product $C = p_{23}p_{32}$ were introduced by Strasser (1978, 1981), with the term "product" denoting that in both cases an energy cycling occurs between the two pigment systems involved.

Model 2 is of lower complexity, assuming light absorption and fluorescence emission by the RC as negligible and adopting the following simplifications concerning conformation: No grouping of the PSII RCs ($k_{bb} = 0$), no migration between the reaction centers of PSII and PSI ($k_{ba} = k_{ab} = 0$) or from PSI to the pigment pools of PSII ($k_{13} = k_{12} = 0$). With these simplifications a RC, after capturing an exciton, can be de-excited by three different pathways, i.e. primary photochemistry $PA \rightarrow P^+A^-$, or energy cycling as back transfer to pigment system **2**, or heat dissipation. Fig. 2 shows the deconvolution of the statistical model 2 into digital models for these three discrete cases which

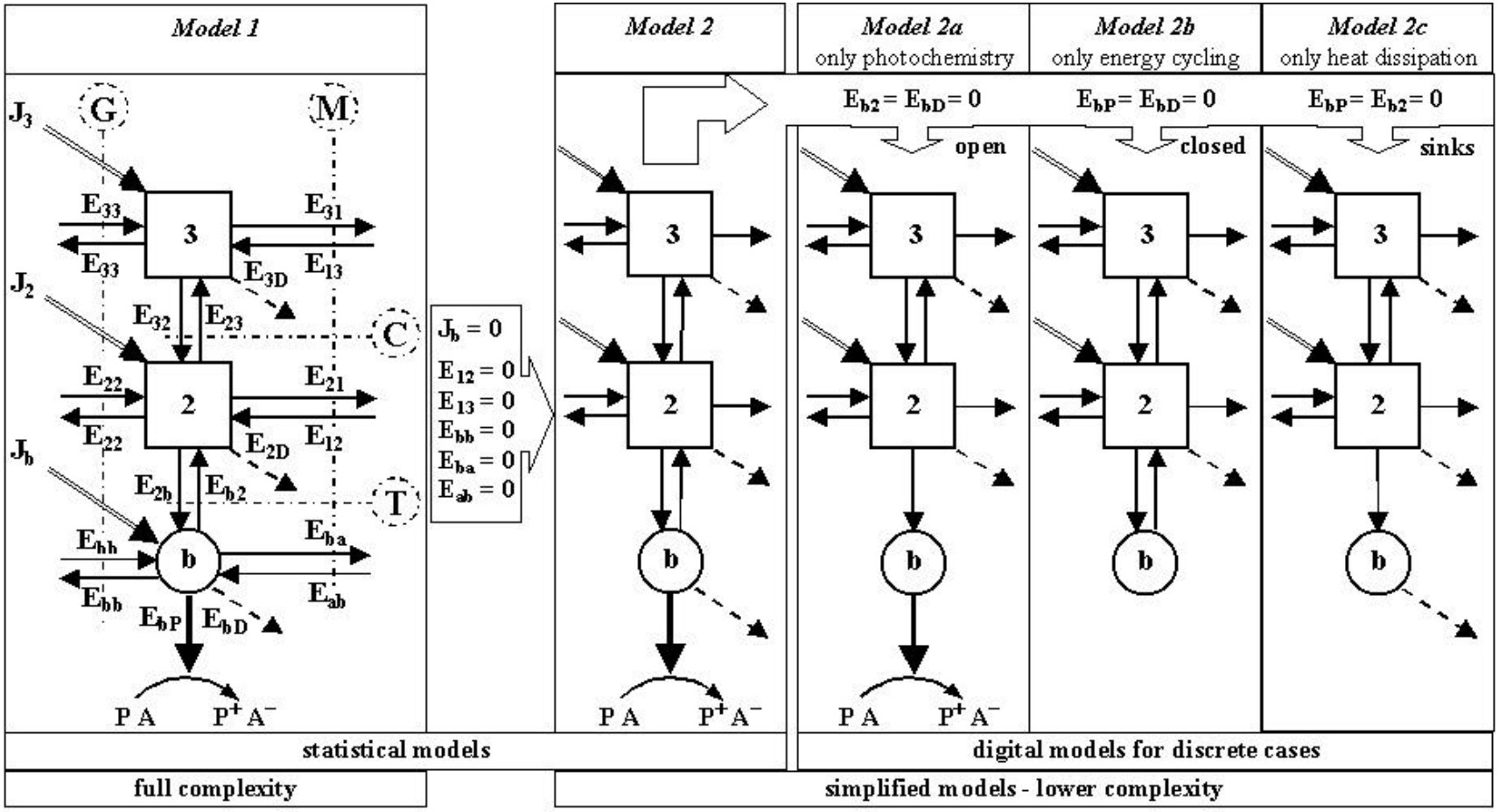
Model 1
Model 2
Model 2a
only photochemistry
Model 2b
only energy cycling
Model 2c
only heat dissipation
G
M
C
T
3
2
b
J3
J2
Jb
E33
E31
E3D
E13
E32
E23
E22
E21
E2D
E12
E2b
Eb2
Ehh
Eba
Ebb
Eab
EbP
EbD
P A
P+A−
Jb = 0
E12 = 0
E13 = 0
Ebb = 0
Eba = 0
Eab = 0
Eb2 = EbD = 0
EbP = EbD = 0
EbP = Eb2 = 0
open
closed
sinks
statistical models
digital models for discrete cases
full complexity
simplified models - lower complexity

Fig. 2. Tripartite models of the photosynthetic apparatus, of high (Model 1) and of lower complexity (Model 2) level. Square and round boxes present pigment pools and RC respectively, while arrows demonstrate energy fluxes. The models assume two pigment systems in PSII (LHC, labeled as **3,** and core antenna, labeled as **2**), channeling finally excitation energy to the PSII reaction center (labeled as **b**), while the PSI pigment systems (not shown) channeling excitation energy to the PSI reaction center (labeled as **a**) are regarded as one site (labeled as **1**). The models assume energy dissipation ($\mathbf{E_{iD} = E_{iH} + E_{iF}}$) by all PSII sites, variable energetic communication between core antenna and RC within a PSII unit (trapping **T**), between core antenna and LHC within a PSII unit (coupling **C**), between same sites of neighbor PSII units (grouping **G**) and between PSII and PSI sites (migration **M**). Models 1 and 2 are statistical models, pooling together units with RCs of different conformation, while model 2 is further deconvoluted into digital models for three discrete conformations of the RC: Model 2a: open RC (only primary photochemistry, $\mathbf{PA® P^{+}A^{-}}$); Model 2b: Closed RC (only energy cycling); Model 2c: Silent RC or heat sink (only heat dissipation).

correspond to different conformation of the RC: Model 2a: Open RC (only primary photochemistry), described by $\mathbf{k}_{b2}^{op} = \mathbf{k}_{bD}^{op} = \mathbf{0} \Rightarrow \mathbf{p}_{bP}^{op} = \mathbf{1}$ and $\mathbf{T}^{op} = \mathbf{0}$. Model 2b: Closed RC (only energy cycling), described by $\mathbf{k}_{bP}^{cl} = \mathbf{k}_{bD}^{cl} = \mathbf{0} \Rightarrow \mathbf{p}_{b2}^{cl} = \mathbf{1}$ and $\mathbf{T}^{cl} = \mathbf{p}_{2b}$. Model 2c: Silent RC or heat sink (only heat dissipation, for the term "silent" see section V.B.2), described by $\mathbf{k_{bP}} = \mathbf{k_{b2}} = \mathbf{0} \Rightarrow \mathbf{p}_{bD}^{si} = \mathbf{1}$ and $\mathbf{T}^{si} = \mathbf{0}$.

The energy flux theory can be applied to formulate any of the models shown in Fig. 2. However, the fluorescence signals provide no information for the distinction between models 1 and 2, neither between these models and the models constructed on the basis of the exciton radical pair (Trissl and Lavergne 1995; Lavergne and Trissl 1995). The variable fluorescence reflects entirely the difference between RCs that conserve energy in primary photochemistry (open), or cycle energy back to core antenna (closed). Hence, we here proceed in an indicative application of the energy flux theory for the two discrete states open and closed of the simplified model 2, denoting by **B** the fraction of closed RCs, while in section V.B.2 we will discuss experimental evidences about the existence of silent RCs and the way to calculate their fraction.

Writing eq. 1 (Table 1) for the two pigment systems and the RC of PSII, gives the following equations' system for the total influxes or excitation rates, where each probability is determined by the appropriate rate constants (see Fig. 2 and eq. 5 in Table 1):

$$\mathbf{E}_3^{op} = \mathbf{J}_3 + (\mathbf{1} - \mathbf{B})\mathbf{E}_3^{op}\mathbf{p}_{33} + \mathbf{B}\mathbf{E}_3^{cl}\mathbf{p}_{33} + \mathbf{E}_2^{op}\mathbf{p}_{23} \qquad \text{(eq. 8)}$$

$$\mathbf{E}_3^{cl} = \mathbf{J}_3 + (\mathbf{1} - \mathbf{B})\mathbf{E}_3^{op}\mathbf{p}_{33} + \mathbf{B}\mathbf{E}_3^{cl}\mathbf{p}_{33} + \mathbf{E}_2^{cl}\mathbf{p}_{23} \qquad \text{(eq. 9)}$$

$$\mathbf{E}_2^{op} = \mathbf{J}_2 + (\mathbf{1} - \mathbf{B})\mathbf{E}_2^{op}\mathbf{p}_{22} + \mathbf{B}\mathbf{E}_2^{cl}\mathbf{p}_{22} + \mathbf{E}_3^{op}\mathbf{p}_{32} \qquad \text{(eq. 10)}$$

$$\mathbf{E}_2^{cl} = \mathbf{J}_2 + (\mathbf{1} - \mathbf{B})\mathbf{E}_2^{op}\mathbf{p}_{22} + \mathbf{B}\mathbf{E}_2^{cl}\mathbf{p}_{22} + \mathbf{E}_b^{cl}\mathbf{p}_{b2}^{cl} + \mathbf{E}_3^{cl}\mathbf{p}_{32} \qquad \text{(eq. 11)}$$

$$\mathbf{E}_b^{op} = \mathbf{E}_2^{op}\mathbf{p}_{2b} \qquad \text{(eq. 12)}$$

$$\mathbf{E}_b^{cl} = \mathbf{E}_2^{cl}\mathbf{p}_{2b} \qquad \text{(eq. 13)}$$

The solution of the equations' system gives the expressions of the total energy influxes for the three PSII sites (**3**, **2** and **b**) at the open and closed state. Concomitantly, all the partial outfluxes within PSII, as well as towards PSI, are derived in terms of the rate constants or probabilities according to eq. 7.

Solving for the energy influxes in the core antenna (pigment system **2**), gives:

(a) at the extremes

The influxes $\mathbf{E}_{2,0}^{op}$ (at the open state when all RCs are open – zero closed) and $\mathbf{E}_{2,M}^{cl}$ (at the closed state when all RCs are closed – maximum closed) are given by the following expressions:

$$\mathbf{E}_{2,0}^{op} = \frac{\mathbf{J}_2 + \mathbf{J}_3\mathbf{p}_{32}/(\mathbf{1} - \mathbf{p}_{33})}{\mathbf{1} - \mathbf{p}_{22} - \mathbf{C}/(\mathbf{1} - \mathbf{p}_{33})} \qquad \text{(eq. 14a)}$$

$$\mathbf{E}_{2,M}^{cl} = \frac{\mathbf{J}_2 + \mathbf{J}_3\mathbf{p}_{32}/(\mathbf{1} - \mathbf{p}_{33})}{\mathbf{1} - \mathbf{p}_{22} - \mathbf{T} - \mathbf{C}/(\mathbf{1} - \mathbf{p}_{33})} \qquad \text{(eq. 14b)}$$

where **T** stands for $\mathbf{T}^{cl}$, the only trapping product different than zero: $\mathbf{T} = \mathbf{p}_{2b}\mathbf{p}_{b2}^{cl} = \mathbf{p}_{2b}$.

(b) At any intermediate redox state between the extremes

The expressions for the energy influxes E_2^{op} and E_2^{cl} and, concomitantly, for the total influxes in all open $E_{2,tot}^{op}$ and all closed units $E_{2,tot}^{cl}$ at any intermediate redox state, i.e. when a fraction **B** of the RCs are closed, are derived as:

$$E_2^{op} = E_{2,0}^{op}\left[\frac{1+C_{HYP}}{1+C_{HYP}(1-B)}\right] \quad \Leftrightarrow \quad E_{2,tot}^{op} = E_{2,0}^{op}\left[\frac{(1+C_{HYP})}{1+C_{HYP}(1-B)}\right](1-B) \qquad \text{(eq. 15a)}$$

$$E_2^{cl} = E_{2,M}^{cl}\left[\frac{1}{1+C_{HYP}(1-B)}\right] \quad \Leftrightarrow \quad E_{2,tot}^{cl} = E_{2,M}^{cl}\left[\frac{1}{1+C_{HYP}(1-B)}\right]B \qquad \text{(eq. 15b)}$$

The magnitude C_{HYP} (curvature constant of the hyperbola V=f(B), see eq. 24 below) is expressed as the product of two terms:

$$C_{HYP} = \left[\frac{E_{2,M}^{cl}}{E_{2,0}^{op}} - 1\right]\left[\frac{1}{1-C}\left(p_{22} + C\frac{p_{33}}{1-p_{33}}\right)\right] \qquad \text{(eq. 16)}$$

The first term is defined only by the energy influxes at the extremes, while the second term contains the probabilities referring to all types of energetic communication among the PSII pigment pools and was denoted by Strasser (1978, 1981) as p_{2G}, the overall-grouping probability for pigment systems **2**:

$$p_{2G} = \frac{1}{1-C}\left(p_{22} + C\frac{p_{33}}{1-p_{33}}\right) \qquad \text{(eq. 17)}$$

Hence,

$$C_{HYP} = \left[\frac{E_{2,M}^{cl}}{E_{2,0}^{op}} - 1\right] p_{2G} \qquad \text{(eq. 18)}$$

Generally defined, the overall-grouping probability p_{iG} is the probability by which an exciton at any site **i** of a pigment bed migrates to the same site **i** in a neighbor unit using all possible migration pathways. Eq. 17 refers to a particular model (model 2 of Fig. 2) and expresses specifically the overall-grouping probability for exciton migration among pigment systems **2**, realized both by a direct transfer **2 ® 2** and a sequential transfer **2 ® 3**, **3 ® 3** and **3 ® 2**. Setting any of the respective probabilities equal to zero leads to a model of lower complexity according to the Grouping Concept (Strasser 1978, 1981), with p_{2G} transformed accordingly (see Fig. 3). However, the splitting of C_{HYP} in two terms, as described by eq. 18, is valid for all possible higher levels of complexity (e.g. model 1 of Fig. 2), with the first term remaining always the same, and the second, i.e. p_{2G}, modified accordingly (see Fig. 3).

Eq. 15a shows that the excitation rate of an open unit is bigger in the presence of closed RCs (**B > 0**) than when all RCs are open (**B = 0**), by the factor **$(1+C_{HYP})/[1+C_{HYP}(1-B)]$**, which was hence called **"**excitation gain factor" (Strasser 1981). The excitation gain factor is equal to 1 for **B = 0** and increases with the increase of **B**. Particular interest must be given to C_{HYP}, since the bigger its value, the bigger the excitation gain is. If both grouping probabilities p_{22} and p_{33} are equal to zero (separate units), C_{HYP} is also equal to zero and the excitation gain factor is equal to 1 independently of the fraction **B** of closed RCs (**0 £ B £ 1**).

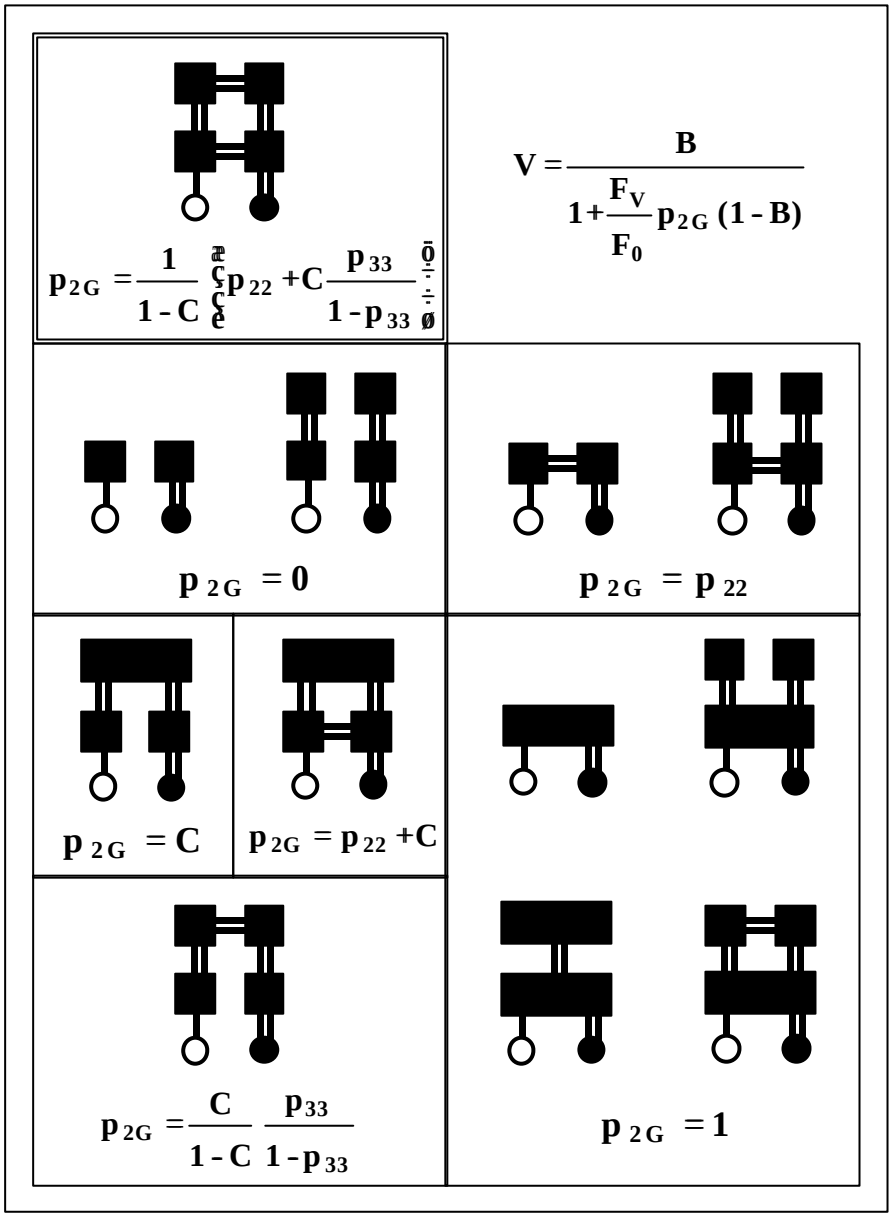

Fig 3. Models of different complexity in respect with architecture of PSII pigment assemblies (small and big units) and variable energetic connectivity (from separate units, $p_{2G}=0$, to fully connected units, $p_{2G}=1$). White and black rounds stand for open and closed RCs respectively and black boxes for pigment pools (2 and 3, see also Fig. 2). The energy cycling between different pigment sites is indicated by a double line joining them, while the "one-way" energy transfer from the antenna site to an open RC is presented by a single line. The function $V = f(B)$ expresses the relation between the relative variable fluorescence and the fraction of closed RCs, valid for all models. The general equation for p_{2G}, derived (see text) for the highest complexity model that assumes variable energetic connectivity (top-left model in a double frame), is valid for all models; it is transformed to specific expressions of p_{2G} for each of the models of lower complexity, by appropriate substitutions of the connectivity rate constants (k_{22} and k_{33}) with zero for no connectivity or infinite for full connectivity. (Based on a figure presented by Strasser 1981).

C. From Biophysical to Experimental Parameters

1. The fluorescence signals

Once the total energy influxes are formulated, the expressions for the fluorescence outfluxes from the core antenna and the LHC, at the open and closed states, are directly derived (eq. 7) by multiplication with the appropriate probability ($\mathbf{p_{2F}}$ or $\mathbf{p_{3F}}$). In the following we assume that the experimental fluorescence signals emerge only from pigment system **2**. Though only a fraction of the fluorescence outfluxes reaches the light detector, the fractional factor can be taken as equal to 1 since the fluorescence intensities are in arbitrary units. Hence, and ignoring for the moment possible influences from the donor side or quenching by oxidized plastoquinone or $P680^+$, the fluorescence signals from open ($\mathbf{F^{op}}$) and closed ($\mathbf{F^{cl}}$) units are written respectively as:

$$\mathbf{F^{op} = E^{op}_{2,tot}\, p_{2F}} \qquad \text{(eq. 19a)}$$

$$\mathbf{F^{cl} = E^{cl}_{2,tot}\, p_{2F}} \qquad \text{(eq. 19b)}$$

(a) at the extremes

The fluorescence emitted when all RCs are open ($\mathbf{F_0}$) or closed ($\mathbf{F_M}$), are written accordingly as:

$$\mathbf{F_0 = E^{op}_{2,0}\, p_{2F}} \qquad \text{(eq. 20a)}$$

$$\mathbf{F_M = E^{cl}_{2,M}\, p_{2F}} \qquad \text{(eq. 20b)}$$

Using eqs. 14a and 14b, the expressions of $\mathbf{F_0}$ and $\mathbf{F_M}$ are derived, in terms of the rate constants (see Fig. 2):

$$\mathbf{F_0 = \frac{J}{k_{2b} + k_{23}(k_{3D} + k_{31})/(k_{32} + k_{31} + k_{3D}) + k_{21} + k_{2D}}\, k_{2F}} \qquad \text{(eq. 21a)}$$

$$\mathbf{F_M = \frac{J}{k_{23}(k_{3D} + k_{31})/(k_{32} + k_{31} + k_{3D}) + k_{21} + k_{2D}}\, k_{2F}} \qquad \text{(eq. 21b)}$$

where **J** is the influx that is solely due to absorbed energy (directly by **2** and through **3**):

$$\mathbf{J = J_2 + J_3 p_{32}/(1 - p_{33}) = J_2 + J_3 k_{32}/(k_{32} + k_{31} + k_{3D})} \qquad \text{(eq. 22)}$$

The terms in the denominator of eq. 21a can be classified in two categories: (a) the rate constant $\mathbf{k_{2b}}$ which, since $\mathbf{p^{op}_{bP} = 1}$, determines primary photochemistry and can be hence written as $\mathbf{k_{2P}}$, (b) terms determining net outfluxes from core antenna, as dissipation $\mathbf{k_{2D} + k_{23}k_{3D}/(k_{32} + k_{31} + k_{3D})}$ and migration $\mathbf{k_{21} + k_{23}k_{31}/(k_{32} + k_{31} + k_{3D})}$, i.e. outfluxes not used for PSII photochemistry; their sum can be hence replaced by an overall rate constant $\mathbf{k_{2N}}$. Thus eqs. 21a and 21b are written as:

$$\mathbf{F_0 = J\frac{k_{2F}}{k_{2P} + k_{2N}}} \qquad \text{(eq. 21a′)}$$

$$F_M = J\frac{k_{2F}}{k_{2N}} \qquad \text{(eq. 21b′)}$$

As shown by eqs. 21a and 21b, F_0 and F_M do not depend on the grouping rate constants k_{22} and k_{33}. This is expected since all units, being at the same redox state, have the same exciton density and, thus, the exchanged energy between any two of them is the same in both directions. Obviously, the same equations can be derived directly from eqs. 8-13, substituting **B = 0** or **B = 1** respectively.

(b) At any intermediate redox state between the extremes

At any intermediate state, the fluorescence of all the open and all the closed units and, concomitantly of the whole illuminated sample, is calculated from eqs. 15, 19 and 20:

$$F^{op} = F_0\frac{(1-B)(1+C_{HYP})}{1+C_{HYP}(1-B)} \qquad \text{(eq. 23a)}$$

$$F^{cl} = F_M\frac{B}{1+C_{HYP}(1-B)} \qquad \text{(eq. 23b)}$$

$$F = F^{op} + F^{cl} = \frac{F_0(1+C_{HYP})(1-B)+F_M B}{1+C_{HYP}(1-B)} = F_0 + (F_M - F_0)\frac{B}{1+C_{HYP}(1-B)} \qquad \text{(eq. 24)}$$

Note that the fluorescence signals F^{op} and F^{cl}, and concomitantly **F**, are functions of **B** which is a function of time **t**.

The second term in eq. 24 is obviously the actual (i.e. at any time during the fluorescence induction) variable fluorescence F_u:

$$F_u = F - F_0 = (F_M - F_0)\frac{B}{1+C_{HYP}(1-B)} \qquad \text{(eq. 25)}$$

Hence, the relative variable fluorescence **V**, defined as the ratio of the variable fluorescence to the maximal variable fluorescence F_V, i.e.

$$V = \frac{F_u}{F_V} = \frac{(F - F_0)}{(F_M - F_0)} \qquad \text{(eq. 26)}$$

is expressed vs. the fraction **B** of closed RCs by the function

$$V = \frac{B}{1+C_{HYP}(1-B)} \qquad \text{(eq. 27)}$$

which is a hyperbola with vertical asymptote. The curvature constant is equal to C_{HYP} (hence the notation in eqs. 15), which, based on eqs. 18 and 20, is written as:

$$C_{HYP} = \left(\frac{F_M}{F_0} - 1\right)p_{2G} = \frac{F_V}{F_0}\,p_{2G} \qquad \text{(eq. 28)}$$

Using eq. 27, eqs. 5 and 23-24 are now written as:

$$E^{op}_{2,tot} = E^{op}_{2,0}(1-V) \qquad \text{(eq. 15a′)}$$

$$E^{cl}_{2,tot} = E^{cl}_{2,M}V \qquad \text{(eq. 15b′)}$$

$$F^{op} = F_0(1-V) \qquad \text{(eq. 23a′)}$$

$$F^{cl} = F_M V \qquad \text{(eq. 23b′)}$$

$$F = F_0 + VF_V \qquad \text{(eq. 24′)}$$

Eqs. 23a′ and 23a′ are very useful for the deconvolution of the fluorescence kinetics into the fluorescence kinetics of open and closed units

2. Experimental vs. theoretical resolution

The above equations were derived on the basis of model 2 (for open and closed RCs only) of Fig. 2 (Strasser 1978, 1981). However, both eq. 27 and the splitting of C_{HYP} in two terms (eqs. 18 and 28) are valid for all possible higher levels of complexity, even further than the tripartite model 1 of Fig. 2, namely for any model with as many pigment complexes and as many different modes of energetic communication among them. Independently of the model, the first term remains always the same, $[(E^{cl}_{2,M}/E^{op}_{2,0}) - 1]$ in biophysical terms (eq. 18) and $[(F_M/F_0)-1]$ in experimental terms (eq. 28), and the second term p_{2G} is modified accordingly. It is worth pointing out that these equations are equivalent to the equations published by all other authors, despite the different way they may appear. In order to get aware of the equivalence with the Joliot's equation (Joliot and Joliot 1964), the first reported one, it has to be taken into account that the apparent differences are due to the consideration at that time that only the variable fluorescence was emitted by PSII. The equivalence with Paillotin's equations (Pailottin 1976), which were derived on the basis of a model where the limited connectivity was realized through the energetic communication of LHCs only (see also Strasser and Butler 1977d), is recognized after rearrangement of the equations. Moreover, the recently published equations on the basis of the exciton radical pair (Trissl and Lavergne 1995; Lavergne and Trissl 1995) are also equivalent with eqs. 27 and 28. The differences, which nevertheless do not affect the equivalence, are restricted to the expression of the probability corresponding to p_{2G}, resulting from the assumptions of the model used, as expected.

On the other hand, eqs. 27 and 28 incorporate the dynamics of the complexity by using variables for the different levels of structure and conformation. Thus, they can describe the behavior and, concomitantly, the activity of the photosynthetic sample under different conditions or different developmental stages resulting in lower complexity, without necessarily adjusting the basic equations 8-13, but only modifying accordingly the derived equations (Fig. 3). For example, in case of small units, i.e. deprived of LHC, as in mutants, or when the complex is phosphorylated and detached (e.g. Tsala and Strasser 1984), or during the development of the photosynthetic apparatus under special conditions (see e.g. Strasser and Butler 1977b; Akoyunoglou 1981; Srivastava et al. 1999), all variables referring to pigment system **3** are set equal to zero (bipartite model). Eqs. 27 and 28 can be used as well for any model of lower complexity concerning the energetic connectivity, between the extreme case of separate units (no grouping, i.e. $p_{22} = 0$ and $p_{33} = 0$) where p_{2G} is equal to zero and thus $V = B$, and the case of full connectivity between **2-2** ($k_{22} = ¥$, lake model) for which $p_{2G} = 1$ and, concomitantly, $C_{HYP} = F_V/F_0$, independently of the extent of the **3-3** grouping. Moreover, any quenching on any pigment system can be taken into account by incorporating in the dissipation rate constants of that system an additional term, equal to the product of the quenching rate constant and the quencher concentration.

However, the experimental resolution is much more limited than the theoretical resolution. For the most common studies, i.e. of mature photosynthetic samples at room temperature, the fluorescence signals do not provide information about distribution of the absorbed energy (J_2 and J_3) in the two pigment complexes. It is neither possible to distinguish between fluorescence emitted by the core antenna and the LHC, nor between their energy dissipation or migration, unless measurements of fluorescence lifetimes are also conducted. Hence, the tripartite model, having a theoretical resolution that becomes meaningless, should be replaced by a bipartite working model that considers core antenna and LHC as one site (labeled as **2**) and we will read the derived equations setting as equal to zero all variables referring to pigment system **3**. In section IV we will go back to the tripartite model since fluorescence signals at low temperature have a more extended resolution. It is worth pointing out that the tripartite model is also useful when studying photosynthetic samples at different

developmental stages (Strasser 1978), from small units (only core antenna) to big units (core antenna and LHC), with gradually increasing complexity regarding conformation.

Actually, the information provided from fluorescence kinetics lead only to the distinction between units with low and high fluorescence yields, which are translated, by agreement, to units with open and closed RCs respectively. However, the further consensus that a RC is closed, i.e. it does not perform photochemistry, when the primary quinone acceptor $\mathbf{Q_A}$ is reduced, is still a dogma as it is not fully supported by experimental evidences; e.g. there is no experimental resolution to distinguish if it is the redox state of $\mathbf{Q_A}$ or of the primary acceptor **Pheo** that defines a closed or open RC. Recognizing this uncertainty, our model is formulated in a more general way, denoting the primary acceptor by **A** (see fig. 2) and avoiding so far to refer to the redox state of $\mathbf{Q_A}$; hence, the derived formulae have a broader validity. Keeping the question open to be discussed in section V.D, we accept in our analysis below the equivalence "open $\Leftrightarrow \mathbf{Q_A}$" and "closed $\Leftrightarrow \mathbf{Q_A^-}$ ", which means that $\mathbf{B = [Q_A^-]/[Q_A^{total}]}$, where $\mathbf{[Q_A^{total}]}$ the total concentration of the bound and reducible quinone.

3. Yields and probabilities

The term "yield" refers to a certain outflux $\mathbf{E_{ix}}$ from a system and is often considered in the literature as synonymous with efficiency. Hence it is defined as the ratio of the particular outflux $\mathbf{E_{ix}}$ to the total energy influx $\mathbf{E_i}$, the latter assumed as equal to the absorbed energy flux $\mathbf{J_i}$. However, as the energy flux theory clearly postulates, $\mathbf{E_i}$ is generally bigger than $\mathbf{J_i}$, due to the energetic communication of different pigment assemblies. Therefore, the yield $\mathbf{j_{ix} = E_{ix}/J_i}$ should be distinguished from the probability $\mathbf{p_{ix} = E_{ix}/E_i}$.

As an example let us consider the fluorescence yields at the extremes, $\mathbf{j_{F_0} = F_0 / J_2}$ and $\mathbf{j_{F_M} = F_M / J_2}$. According to eqs. 21a and 21b, and with $\mathbf{J=J_2}$ (see above), the yields are given as ratios of the fluorescence rate constant $\mathbf{k_{2F}}$ to sums of rate constants that describe net outfluxes, written according to eqs. 21a′ and 21b′ as $\mathbf{j_{F_0} = k_{2F} /(k_{2P} + k_{2N})}$ and $\mathbf{j_{F_M} = k_{2F} / k_{2N}}$ respectively. Hence, they are completely different than the fluorescence emission probability $\mathbf{p_{2F}}$, which is the ratio of $\mathbf{k_{2F}}$ to the sum of all rate constants describing all energy outfluxes from pigment system **2** (see eq. 5 in Table 1).

4. The quantum yield for primary photochemistry

According to the clarification made above for fluorescence yields, the quantum yield for primary photochemistry $\mathbf{j_P}$ is defined as the ratio of the total energy flux trapped by the PSII RCs and used for primary photochemistry, $\mathbf{(1-B)E_b^{op}p_{bP}^{op} = E_{2,tot}^{op}p_{2b}p_{bP}^{op}}$, to the influx $\mathbf{J_2}$. Taking into account that $\mathbf{p_{bP}^{op} = 1}$ and recalling eq. 15a′ we get:

$$\mathbf{j_P = E_{2,tot}^{op}p_{2b} / J_2 = (E_{2,0}^{op}p_{2b} / J_2)(1-V) = (j_{Po})(1-V)} \qquad \text{(eq. 29)}$$

$\mathbf{j_{Po}}$ is the maximum quantum yield of primary photochemistry (when all RCs are open, $\mathbf{V=0}$):

$$\mathbf{j_{Po} = \frac{E_{2,0}^{op}p_{2b}}{J_2} = \frac{p_{2b}}{1-p_{22}} = \frac{k_{2b}}{k_{2b}+k_{21}+k_{2D}} = \frac{k_{2P}}{k_{2P}+k_{2N}} = 1 - \frac{k_{2N}}{k_{2P}+k_{2N}}} \qquad \text{(eq. 30)}$$

Correlating eq. 30 with eqs. 21a′ and 21b′, gives:

$$\mathbf{j_{Po} = 1 - \frac{F_0}{F_M} = \frac{F_V}{F_M}} \qquad \text{(eq. 30′)}$$

Hence, eq. 29 is re-written as

$$j_P = [j_{Po}][1 - V] = \left[\frac{F_V}{F_M}\right]\left[1 - \frac{F - F_0}{F_M - F_0}\right] \quad \Rightarrow \qquad \text{(eq. 31)}$$

$$j_P = \frac{F_M - F}{F_M} \qquad \text{(eq. 32)}$$

It is worth reminding here the "history" of the above equations. Eq. 30′ is the well-known Butler's formula (Kitajima and Butler 1975), derived both for the case of separate units and for the lake models, i.e. the completely connected units (called in that report as "matrix"). Paillotin (1976) derived equation $j_P = j_{Po}\,[(F_M\text{-}F)/(F_M\text{-}F_0)]$ (written here, for comparison, with the symbols we use). Applying the theory of energy fluxes, Strasser (1978) derived the equations 29 to 32, as above presented. Note that the expression in brackets in Paillotin's equation is identical to **(1-V)**; moreover, it is identical with the so-called photochemical quenching qQ, as defined for the steady state of the Kautsky transient, i.e. at F=Fs. Hence, Genty's equation $j_e = DF/F_M$ (Genty et al. 1989) for the quantum yield of electron transport, which is equal to the quantum yield of primary photochemistry (since it refers to the steady state), is obviously identical to eq. 32.

III. Fluorescence Transients in the Presence of Diuron at Room Temperature

The redox state of Q_A, the primary quinone acceptor of PSII, is determined by its photochemical reduction due to PSII activity and its re-oxidation by the electron transport driven by PSI activity. In order to reduce the complexity of the *in vivo* system and facilitate the investigation of PSII properties, the utilization of diuron (DCMU), an inhibitor of the electron flow further than Q_A^-, has been widely employed. In the presence of DCMU at room temperature, the fluorescence kinetics reflects pure photochemical events leading to the complete reduction of Q_A (full closure of RCs). Hence, the maximal recorded fluorescence F_P is equal to F_M. Under normal conditions Q_A is assumed to be completely oxidized in the dark, i.e. all RCs re-open, and the fluorescence signal at the onset of illumination is F_0. From the fluorescence values at the extremes, the value of the maximum yield of primary photochemistry is calculated: $j_{Po} = 1-(F_0/F_M) = F_V/F_M$

The fluorescence induction curve can be deconvoluted into the fluorescence kinetics of open and that of closed RCs, according to eqs. 23a′ and 23b′. It is very useful that this deconvolution is permitted (a) independently of whether the PSII units are energetically separated or connected and, (b) not only in DCMU-treated samples, but under any physiological condition provided that the extremes F_0 and F_M can be experimentally determined.

Further analysis of the fluorescence kinetics in the presence of DCMU gives the following information:

A. The Area above the Fluorescence Transient

The rate of Q_A reduction in the presence of DCMU is written according to the above presented theory and model as:

$$d[Q_A^-]/dt = [Q_A]E_b^{op} = [Q_A]E_2^{op}p_{2b}p_{bP}^{op} = [Q_A]E_2^{op}p_{2b} \qquad \text{(eq. 33)}$$

Dividing by the total concentration of the quinone, $[Q_A^{total}]$, eq. 33 gives (see also eq. 29):

$$dB/dt = (1 - B)E_2^{op}p_{2b} = E_{2,tot}^{op}p_{2b} = J_2 j_P = J_2 j_{Po}(1 - V) \qquad \text{(eq. 33′)}$$

Hence, the fraction of closed centers **B** at any time **t** is linked with the experimental fluorescence transient as follows:

$$B = \int_0^B dB = \int_0^t (dB/dt)\,dt = J_2\, j_{Po} \int_0^t (1 - V)\,dt \qquad \text{(eq. 34)}$$

The integral $\int_0^t (1 - V)\,dt$ is the area between the fluorescence transient plotted as **V=f(t)**, the horizontal line at $F=F_M$ and the vertical line at time **t**, called the complementary area s_t.
For $t \to \infty$ (practically until $t = t_{F_M}$ when F_M is achieved and **V=1**) the integral is the total complementary area s_{max} and **B** equals unity:

$$1 = J_2 \, j_{Po} \int_0^{t\to\infty} (1 - V)\,dt \qquad \text{(eq. 34′)}$$

Hence,

$$B_{(t)} = \left[\int_0^t (1 - V)\,dt\right] \Big/ \left[\int_0^{t\to\infty} (1 - V)\,dt\right] = \frac{s_t}{s_{max}} \equiv S_{(t)} \qquad \text{(eq. 35)}$$

where **S** is the complementary area normalized on the total.

The equality **B=S**, derived from the general model, is valid independently of the energetic connectivity between the units, from separate to lake-type units.

Obviously, $S_{(t)}$ can be calculated from the complementary area until time **t** (denoted as $Area_{(t)}$) and the total complementary area (**Area**) of the directly recorded transient **F=f(t)**:

$$Area_{(t)} = \int_0^t (F_M - F_t)\,dt = (F_M - F_0)\int_0^t (1 - V)\,dt \qquad \text{(eq. 36)}$$

$$Area = \int_0^{t_{F\,max}} (F_M - F_t)\,dt = (F_M - F_0)\int_0^{t_{F\,max}} (1 - V_t)\,dt \qquad \text{(eq. 36′)}$$

$$Area_{(t)} / Area = \left[\int_0^t (1 - V)\,dt\right] \Big/ \left[\int_0^{t\to\infty} (1 - V)\,dt\right] = S_{(t)} \qquad \text{(eq. 37)}$$

B. The Shape of the Fluorescence Transient

The observation of a sigmoidal shape instead of the exponential expected for separate units, led Joliot and Joliot (1964) to the theory of energetic connectivity. Strasser (1978, 1981) and several other authors since then (e.g. Trissl and Lavergne 1995; Stirbet et al. 1998; Strasser and Stirbet 2001) presented and mathematically analyzed sigmoidal transients.

The derivation of the mathematical formulation of the fluorescence transient is as follows:

Using eq. 27, eq. 33 is re-written as

$$dB/dt = J_2 \, j_{Po} \frac{(1 - B)(C_{HYP} + 1)}{1 + C_{HYP}(1 - B)} \qquad \text{(eq. 38)}$$

and gives, by integration the **t=f(B)** equation:

$$t = \frac{1}{J_2 \, j_{Po} (C_{HYP} + 1)} \left\{ - \ln(1 - B) + C_{HYP} B \right\} \qquad \text{(eq. 39)}$$

Substitution of **B** from eq. 27, gives equation **t=f(V)**, which expresses the sigmoidal shape of **V=f(t)**:

$$t = \frac{1}{J_2 \, j_{Po} (C_{HYP} + 1)} \left[- \ln \frac{1 - V}{1 + V C_{HYP}} + \frac{C_{HYP}(C_{HYP} + 1) V}{1 + V C_{HYP}} \right] \qquad \text{(eq. 40)}$$

For separate units, with $C_{HYP}=0$ and **V=B**, eq. 39 and eq. 40 become identical, and **V=B=f(t)** degenerates to exponential:

$$V = B = 1 - \exp(-J_2 \, j_{Po} \, t) \qquad \text{(eq. 41)}$$

C. Determination of the Over-All Grouping Probability

Comparing transients from DCMU-treated samples with different degrees of grouping, it is expected that the higher the value of the curvature constant C_{HYP}, the more pronounced the sigmoidal shape of **V = f(t)** is. However, this is qualitative information. Moreover, when C_{HYP} is smaller than a threshold value, the transient does not show the typical inflection point visually characterizing a sigmoidicity, though it deviates from the exponential shape. It has to be emphasized that C_{HYP} and, consequently, the sigmoidicity of **V=f(t)**, depends both on the extent of the grouping probability and on the ratio F_V/F_0 (eq. 28). For example, when a dark adapted and a light adapted photosynthetic sample are compared in respect to the energetic connectivity they exhibit, it has to be taken into account that the former has a much higher F_V/F_0 ratio than the latter. Furthermore, it has to be emphasized that the overall grouping probability depends not only on the rate constants for grouping but on the whole set of rate constants. Hence, the conclusion often found in the literature that an increase of C_{HYP} indicates that the photosynthetic units come physically closer to one another (increase of k_{22} or k_{33}) is an over-estimation of the information that the experimental signals can provide.

For quantitative information, simulations of the transient were recently used (see below). However, 20 years ago Strasser showed a simple way to detect grouping and calculate the over-all grouping probability in DCMU-treated samples (Strasser 1981):

The experimentally determined relative variable fluorescence $V = (F-F_0)/(F_M-F_0)$ and the fraction of closed centers **B = S** are plotted in a **V** vs. **B** graph. If the units are energetically connected, eq. 27 predicts that **V = f(B)** is a hyperbola with a vertical asymptote, which degenerates to a straight line **V = B** (0,0 to 1,1) only in the case of isolated units. Further than detecting the existence of grouping and, even, deducing which curve has bigger C_{HYP} constant by comparing the extent of deviation of **V=f(B)** from the straight line, quantitative information is provided by plotting **B/V** vs. **B**, which gives a straight line, in accordance with the equation:

$$B / V = (1 + C_{HYP}) - C_{HYP} \times B \qquad \text{(eq. 42)}$$

The slope gives the value of C_{HYP}, from which the overall grouping probability is calculated according to eq. 28, since F_V/F_0 is already experimentally accessed (for details see Strasser et al. 1997; Strasser and Tsimilli-Michael 2001).

In practice **V** vs. **B** is never a pure hyperbolic function, since a heterogeneous mixture of different types of units, i.e. big grouped, big separate and small separate units, is always present. An appropriate deconvolution of the experimentally measured induction curve (Strasser 1978) into **V** vs. **B** for each type separately enables not only to distinguish but as well to estimate the fractions of the different types in the mixture. It is, therefore, possible to follow, through the fluorescence signals above described, the changes in respect to the energetic connectivity and the heterogeneity that the photosynthetic apparatus, depending on its developmental stage, may undergo upon environmental changes in order to adapt to new conditions. For example, experimentally investigated fluorescence kinetics in the presence of DCMU were found to change from the exponential shape demonstrating the behavior of separate units, which was observed under low salt conditions, to a sigmoidal shape observed under high salt conditions that favor the grouping of the units (Strasser 1978).

IV. Fluorescence Transients at Low Temperature

The fluorescence emission spectra at low temperature show three or more emission bands, which have been attributed to distinct pigment complexes: The long wavelength band, exhibited at 725 nm by young plants and flashed leaves, at 735 nm by mature chloroplasts of higher plants and at about 715 nm by many green algae, is attributed to PSI (core and peripheral antenna), except for a small fraction which is due to the long wavelength tail of the 695 nm emission band (see e.g. Strasser and Butler 1977c). The 695 nm band is known to originate from the core antenna of PSII and the band at 685 nm from the LHC *a/b*. Hence, the fluorescence transients recorded at these three wavelengths can provide information for the three complexes accordingly (tripartite model).

A. The Fluorescence Transient at 695 nm

The approach described in section III utilizes the fact that, in the presence of DCMU at room temperature, the experimental fluorescence induction curve reveals the kinetics of the pure photochemical closure of the RCs leveling off at $\mathbf{F_M}$. It would therefore be expected that the same analysis could be applied when the electron transport flux is inhibited by low temperature (77 K). However, the fluorescence transient at 695 nm (emitted by the PSII core antenna) never shows a sigmoidal shape (Butler 1978) and the plot of the relative variable fluorescence $\mathbf{V_L}$ vs. the normalized complementary area $\mathbf{S_L}$ (subscript "L" indicating low temperature) is a hyperbola with a horizontal asymptote and a curvature that decreases when grouping increases (Strasser 1978; Strasser and Greppin 1981). A theoretical model was proposed to explain this discrepancy, predicting that at low temperature the fraction of closed RCs is not equal to the normalized complementary area but their relation $\mathbf{B_L = f(S_L)}$ is a horizontal hyperbola; the prediction was based on arguments that at 77 K one RC reduces in multiple turn over events not only one, but a pool of electron acceptors (Strasser, 1978; Strasser and Greppin, 1981). The analytical formulation of the model permits the calculation of the equilibrium constant of the donor-acceptor reaction, as well as of the overall grouping probability in good agreement with the values calculated from DCMU-treated samples at ambient temperature (Strasser and Greppin 1981; for details see also Strasser et al. 1997).

B. Correlation of Fluorescence Transients at 685 nm, 695 nm and 735 nm

The fluorescence transients at 685 nm, 695 nm and 735 nm have the same shape, though with different values of the $\mathbf{F_0/F_M}$ ratio. For mature green leaves it was moreover shown that at low temperature the excitation spectra of the initial fluorescence at 695 nm, the variable fluorescence at 695 and the variable fluorescence at 735 nm are all identical, while the excitation spectrum of the initial fluorescence at 735 nm is different (Strasser and Butler 1977a, 1977b). This means that the redox state of PSI reaction center does not affect the fluorescence emission and that the origin of the PSI variable fluorescence are the PSII redox state changes, which define the PSII exciton density and, concomitantly, the migration flux to PSI. However, there are cases where part of the PSI variable fluorescence is due to photo-oxidation of P700, for example in red algae (Ley and Butler 1977), *Chlamydomona*s (R.J. Strasser, unpublished) and cyanobacteria (Karapetyan et al. 1999).

Clear evidence about the origin of the PSI variable fluorescence is provided by simultaneous measurements of the fluorescence induction kinetics $\mathbf{F_1=f(t)}$ and $\mathbf{F_2=f(t)}$ at 735 and 695 nm respectively, and the plotting of $\mathbf{F_1}$ vs. $\mathbf{F_2}$. Assuming a bipartite model (Strasser and Butler 1976, 1977b) and applying the energy flux theory gives:

$$\mathbf{F_1 = J_1\, p_{1F} + F_2\, (k_{21} / k_{2F})\, p_{1F}} \qquad \text{(eq. 43)}$$

Hence, if $\mathbf{F_1=f(F_2)}$ is a straight line, the PSI variable fluorescence originates solely from PSII, while any deviation from the straight line indicates that the redox state of P700 is also involved (see e.g. Ley and Butler, 1977).

The plot $\mathbf{F_1=f(F_2)}$ is also very useful for the comparison of photosynthetic samples at different conditions. For example, under conditions of LHC phosphorylation, the intercept of $\mathbf{F_1}$ vs. $\mathbf{F_2}$ was found to increase while the slope remained unchanged (Butler and Strasser 1977b; Tsala and Strasser 1984). In terms of eq. 43, the intercept increase is in accordance with the "movement" of the phosphorylated complex towards PSI and the concomitant increase of $\mathbf{J_1}$, while the slope insensitivity indicates that the migration rate constant $\mathbf{k_{21}}$ is not affected. On the other hand, high salt (Mg^{++}) conditions, compared to low salt, resulted in a decrease of the slope of the $\mathbf{F_1}$ vs. $\mathbf{F_2}$ graph, indicating that $\mathbf{k_{21}}$ decreases, in accordance with the parallel increase of $\mathbf{F_V/F_M}$ (Tsala and Strasser 1984); the indications for energy migration from PSII to PSI (spill-over) were confirmed by simultaneous measurements of the photo-oxidation of P700.

A further utilization of the fluorescence signals at low temperature is possible, since their resolution, contrary to measurements at room temperature, corresponds to the theoretical resolution of the tripartite model. Solving the basic equations derived for this model (Fig. 2) and with the notations $\mathbf{F_1}$, $\mathbf{F_2}$ and $\mathbf{F_3}$ for the fluorescence emitted at 735 nm (PSI), 695 nm (PSII core antenna) and 685 nm (PSII LHC) respectively, gives the following relations $\mathbf{F_3=f(F_2)}$, $\mathbf{F_1=f(F_2)}$ and $\mathbf{F_1=f(F_3)}$:

$$F_3 = J_3 p_{3F} + F_2 \frac{k_{23}}{k_{2F}} p_{3F} \qquad \text{(eq. 44)}$$

$$F_1 = \left[J_1 + J_3 \frac{p_{31}}{1 - p_{33}} \right] p_{1F} + F_2 \left[\frac{k_{21}}{k_{2F}} + \frac{k_{23} p_{31}}{k_{2F} (1 - p_{33})} \right] p_{1F} \qquad \text{(eq. 45)}$$

$$F_1 = \left[J_1 - J_3 \frac{k_{21}}{k_{23}} \right] p_{1F} + F_3 \left[\frac{k_{21}}{k_{23}} + \frac{p_{31}}{1 - p_{33}} \right] \frac{p_{1F}}{p_{3F}} \qquad \text{(eq. 46)}$$

According to eqs. 44-46, the plot of any two of the three fluorescence fluxes is expected to be a straight line. This was indeed verified experimentally (Strasser and Butler 1977c; Strasser 1986) when fluorescence induction kinetics simultaneously measured at the three mentioned wavelengths, $\mathbf{F_1=f(t)}$, $\mathbf{F_2=f(t)}$ and $\mathbf{F_3=f(t)}$, were used to plot $\mathbf{F_3=f(F_2)}$, $\mathbf{F_1=f(F_2)}$ and $\mathbf{F_1=f(F_3)}$. The intercepts and slopes provide information about the absorption criteria of the three pigment complexes and the probabilities and/or rate constants of the energy transfer fluxes among them (Strasser et al. 1997; Strasser and Tsimilli-Michael 2001).

V. Polyphasic Fluorescence Transients in Vivo

The fluorescence measurements at room temperature and in the presence of DCMU or at low temperature give a lot of information about the energy distribution in the sample as it is at the time before treatment. A living system however emits all the time whenever it is excited and the emission carries the whole energetic information about the system. The well known fluorescence induction curve in vivo, first observed by Kautsky and Hirsch (1931), shows an initial rise O-P lasting for less than 1 s up to several seconds depending on the actinic light intensity, and a subsequent decrease P-S occurring in the time range of seconds to minutes with several intermediate steps (see also Fig. 1). The O-P part of the transient is accepted to reflect the closure of RCs (accepted as equivalent to the reduction of $\mathbf{Q_A}$) and no conformational changes, i.e. no changes of de-excitation rate constants of the antenna chlorophyll are assumed to occur in this short time. The P-S part of the transient reflects both a state transition, i.e. conformational changes induced by prolongation of the illumination and affecting one or several de-excitation rate constants, and changes of the fraction of closed RCs.

It has been recognized, already 34 years ago (Delosme 1967) that the O-P fluorescence rise is not monophasic. Several reports since then presented one or two intermediate between O and P (Munday and Govindjee 1969; Neubauer and Schreiber 1987; for reviews see Papageorgiou 1975; Krause and Weis 1991). However, the detailed shape of the polyphasic fluorescence transient over a wide time range was revealed only when the fluorescence signals were recorded with a high time-resolution instrument, namely the PEA-fluorimeter (Plant Efficiency Analyser, built by Hansatech Instruments Ltd. King's Lynn Norfolk, PE 30 4NE, GB) which provides a very low noise data acquisition every 10 μs for the first 2 ms and every 1 ms thereafter, and were plotted on a logarithmic time scale (Strasser and Govindjee 1992a, 1992b; Strasser et al. 1995). Under high-intensity continuous actinic light (above 200 W m^{-2}) the fluorescence rise exhibits usually the steps J (at 2 ms) and I (at about 20-30 ms) between the initial O (F_0) and the maximum P (F_P), hence labeled as O-J-I-P (Fig. 4). More steps were also observed in certain cases and labeled following an

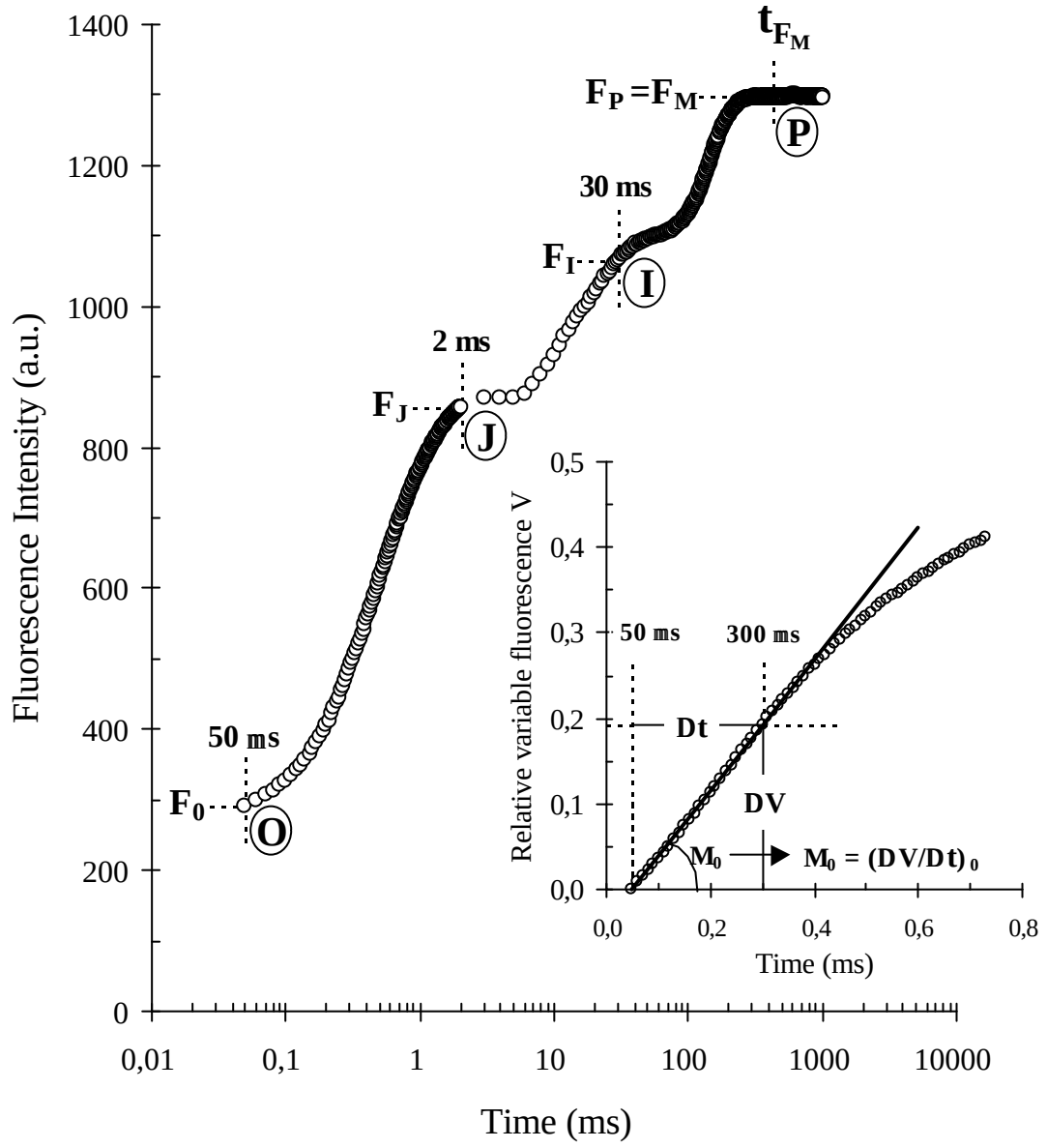

Fig. 4. A typical Chl *a* polyphasic fluorescence rise O-J-I-P, exhibited by higher plants. The transient is plotted on a logarithmic time scale from 50 μs to 1 s. The marks refer to the selected fluorescence data used by the JIP-test for the calculation of structural and functional parameters. The signals are: the fluorescence intensity F_0 (at 50 μs); the fluorescence intensities $\mathbf{F_J}$ (at 2 ms) and $\mathbf{F_I}$ (at 30 ms); the maximal fluorescence intensity, $\mathbf{F_P = F_M}$ (at $\mathbf{t_{F_M}}$). The insert presents the transient expressed as the relative variable fluorescence $\mathbf{V = (F-F_0)/(F_M-F_0)}$ vs. time, from 50 μs to 1 ms on a linear time scale, demonstrating how the initial slope, also used by the JIP-test, is calculated: $\mathbf{M_0 = (dV/dt)_0 @ (DV/Dt)_0 = (V_{300ms})/(0{,}25\ ms)}$. (From Tsimilli-Michael et al. 2000).

alphabetic order (from the latest to the earliest), like the K-step (see below), or the H- and G-steps in corals and foraminifers (Tsimilli-Michael et al., 1998; 1999), while any step, depending on the conditions, can be the highest, i.e. the P-step. Potentially every step can be followed by a temporary fluorescence decrease - dip, e.g. D_K, D_J, D_I etc., and the full transient is hence denoted as O-K-D_K-J-D_J-I-D_I-H-D_H-G-D_G-…S.

In the frame of the present paper we choose not to include aspects and theoretical approaches of state changes either occurring during the P-S polyphasic decline or induced by stress (see e.g. Strasser 1985, 1988; Tsimilli-Michael et al. 1996; Tsimilli-Michael and Strasser 2001), and we focus on experimental methods that enable their study. Such a method (Lombard and Strasser, 1984) is presented in section A below for the investigation of the state 1 to state 2 transition (P-S decline). Moreover, all methods presented in the further sections can be used to provide adequate information about the structure, conformation and function of the photosynthetic apparatus at any moment during the state transition P-S (see Fig. 6 below) and, more generally, at any state induced by any stress (Strasser et al. 2000).

A. Simultaneous Kautsky transients at two wavelengths

Contrary to the case of low temperature (see section IV), no distinct bands corresponding to PSI and PSII appear in the fluorescence emission spectra at room temperature. However, the following method was established (Lombard and Strasser 1984), providing information about the excitation rate of the two photosystems at room temperature:

The investigation of the fluorescence emission spectra in whole leaves at different times during the P-S transitions showed that, besides the decreasing of their peak value (at 685 nm), a change of their shape was also developing. This change, revealed when the spectra were normalized each on its peak value, was a small but clear increase in the longer wavelength region of the spectra. This observation is the basis of the method. Plotting the difference of the normalized spectra showed that the increase had its maximal value at about 715 nm. It was assumed that the experimentally measured fluorescence signal at 685 nm, $\mathbf{F_{685}^{exp}}$, is emitted solely by PSII, while the experimentally measured fluorescence signal at 715 nm, $\mathbf{F_{715}^{exp}}$, originates from both photosystems:

$$\mathbf{F_{685}^{exp} = F_{2(685)}} \qquad \text{(eq. 47a)}$$

$$\mathbf{F_{715}^{exp} = F_{1(715)} + F_{2(715)} = F_{1(715)} + a.F_{685}^{exp}} \qquad \text{(eq. 47b)}$$

where $\mathbf{a}$ is an intrinsic proportionality factor.

According to the energy flux theory (see also application in section IV.B):

$$\mathbf{F_{1(715)} = J_1\, p_{1F} + F_{685}^{exp}(k_{21}/k_{2F})\, p_{1F}} \qquad \text{(eq. 48)}$$

Hence, eq. 47b gives:

$$\mathbf{F_{715}^{exp} = J_1\, p_{1F} + F_{685}^{exp}[a + (k_{21}/k_{2F})\, p_{1F}]} \qquad \text{(eq. 49)}$$

Eq. 49 describes a straight line (similarly to eq. 43 for low temperature). Measurements of the fast fluorescence rise at the two wavelengths at different stages of a P-S transition (state 1 to state 2 transition) showed that for each stage between P and S the $\mathbf{F_{715}^{exp}}$ vs. $\mathbf{F_{685}^{exp}}$ plot was a straight line, and that both the slope and the intercept of the lines were increasing with the advancement of the P-S transition. This means that both a change in the incident energy distribution in favor of PSI ($\mathbf{J_1}$ increase), indicating a progressing phosphorylation of the LHC, and an increase of spill-over ($\mathbf{k_{21}}$) is occurring (see also section IV.B). Performing the same experiment with chloroplasts under

phosphorylating conditions no change of the intercept was observed, which further supports the validity of the method.

The same theoretical approach was used for the comparison of simultaneously recorded fluorescence transients induced by change of the quality of actinic light from red, which enhances PSI excitation and hence establishes state 1, to blue, which preferentially excites PSII leading to state 2. In this case, the criterion was the $\mathbf{F_{715}^{exp}/F_{685}^{exp}}$ ratio, which, according to eq. 49 and substituting $\mathbf{J_1=0}$, is given as:

$$\frac{\mathbf{F_{715}^{exp}}}{\mathbf{F_{685}^{exp}}} = \mathbf{(k_{21}/k_{2F})\ p_{1F}} \qquad \text{(eq. 49′)}$$

It was found that this ratio is increasing during the state 1 to state 2 transition, indicating an increasing spill-over rate constant, while a decrease was observed during the F_0 to F_P rise.

It was further found that the extent of the changes depends on the ability of the sample to adapt to variations of light conditions, which is modified when the sample is exposed to stress. Hence a stress-adaptation-index was defined, $\mathbf{A_{Ps}}$ or $\mathbf{A_{Po}}$, which uses the fluorescence signals $\mathbf{F_P}$ and $\mathbf{F_S}$ or $\mathbf{F_0}$ and $\mathbf{F_P}$ respectively, at both wavelengths (Strasser et al. 1987, 1988):

$$\mathbf{A_{Ps} = 1 - \frac{F_{P(715)}/F_{P(685)}}{F_{S(715)}/F_{S(685)}}} \qquad \text{(eq. 50a)}$$

$$\mathbf{A_{Po} = 1 - \frac{F_{P(715)}/F_{P(685)}}{F_{0(715)}/F_{0(685)}}} \qquad \text{(eq. 50b)}$$

These indexes are very sensitive to stress conditions and were proven to be very useful for early diagnosis of stress (Strasser et al. 1987, 1988).

B. The JIP-test as a tool for fast in vivo vitality screenings

The polyphasic fluorescence rise is widely accepted to reflect the accumulation of the reduced form of the primary quinone acceptor $\mathbf{Q_A}$ (i.e. the RCs' closure), which is the net result of $\mathbf{Q_A}$ reduction due to PSII activity and $\mathbf{Q_A^-}$ reoxidation due to PSI activity. It is assumed that under normal conditions $\mathbf{Q_A}$ is completely oxidized in the dark, i.e. all RCs re-open, and the fluorescence signal at the onset of illumination is $\mathbf{F_0}$. The maximum yield $\mathbf{F_P}$ depends on the achieved reduction-oxidation balance and acquires its maximum possible value, $\mathbf{F_M}$, if the illumination is strong enough (above 100 W m^{-2}) to ensure the closure of all RCs. A lot of information has been driven during the last seventy years from the fluorescence transient (see e.g. Krause and Weis 1991; Govindjee 1995). Transients recorded with high time-resolution fluorimeters, e.g. with the PEA-instrument (or its recent version, the Handy-PEA), have provided additional and/or more accurate information (Strasser and Govindjee 1992a, 1992b; Strasser et al. 1995), namely a precise detection of the initial fluorescence $\mathbf{F_0}$ even in the presence of DCMU, of the initial slope - which offers a link to the maximum rate of primary photochemistry per RC - and of the amplitude and appearance time of the intermediate steps. Moreover, the fully digitized fluorescence kinetics allow further detailed analysis, e.g. different normalizations, calculation of kinetics differences as well as of time-derivatives.

All oxygenic photosynthetic material investigated so far using this method show the polyphasic rise with the basic steps O-J-I-P (Fig. 4), with minor differences among different phenotypes. The shape of the O-J-I-P transient has been found to be very sensitive to stress caused by changes in different environmental conditions, e.g. light intensity, temperature, drought, atmospheric CO_2 or ozone

elevation and chemical influences (see e.g. Srivastava and Strasser 1995, 1996, 1997; Tsimilli-Michael et al. 1995, 1996, 1999, 2000; Van Rensburg et al. 1996; Krüger et al. 1997; Ouzounidou et al. 1997; Clark et al. 1998, 2000).

A quantitative analysis of the O-J-I-P transient has been introduced (Strasser and Strasser 1995) and further developed (for a review see Strasser et al. 1999, 2000), named as the "JIP-test" after the basic steps of the transient, by which several phenomenological and biophysical - structural and functional - parameters quantifying the PSII behavior are calculated. The JIP-test was proven to be a very useful tool for the in vivo investigation of the adaptive behavior of the photosynthetic apparatus and, especially, of PSII to a wide variety and combination of stressors, as it translates the shape changes of the O-J-I-P transient to quantitative changes of the several parameters (see also Strasser and Tsimilli-Michael 2001; Tsimilli-Michael and Strasser 2001).

The JIP-test aims to serve as a tool for in vivo vitality screenings in biotechnology, fruit and vegetable post-harvest quality controls and in environmental analytics. To be useful and practical, the test has to be easy, fast and allowing testing of any type of chlorophyll containing samples in any form and in a short time (over 200 samples can be tested in a working hour per instrument). Therefore, reasonable compromises had to be decided and several expressions have been redefined and relabeled to distinguished from the rigorously defined biophysical expressions.

The JIP-test applies to transients induced by strong actinic light that ensures $\mathbf{F_P = F_M}$. The maximal intensity of red light (peak at 650 nm) provided by the light source of the PEA or Handy-PEA-fluorimeter (an array of six or three light emitting diodes respectively), is routinely used. The JIP-test exploits, besides $\mathbf{F_M}$, the following values extracted from the data stored during the first second (see Fig. 4): the fluorescence intensity at 50 μs (with the PEA-fluorimeter) or 20 μs (with the Handy-PEA-fluorimeter) considered to be $\mathbf{F_0}$; the fluorescence intensity at 100 μs and 300 μs, at 2 ms (denoted as $\mathbf{F_J}$) and at 30 ms (denoted as $\mathbf{F_I}$); the time $\mathbf{t_{F_M}}$ to reach $\mathbf{F_M}$; the total complementary area, denoted as "**Area**", between the fluorescence transient and the line $\mathbf{F = F_M}$.

1. Fluxes and yields

The energy cascade from PSII light absorption to electron transport is shown in the simplified scheme of Fig. 5 (based on a scheme by Strasser and Strasser 1995). **ABS** refers to the photon flux absorbed by the antenna pigments and creating excited chlorophyll, **Chl***. Part of the excitation energy is dissipated, mainly as heat and less as fluorescence emission **F**, and another part is channeled as trapping flux **TR** to the reaction center to be converted to redox energy by reducing the electron acceptor $\mathbf{Q_A}$ to $\mathbf{Q_A^-}$**,** which is then re-oxidized to $\mathbf{Q_A}$ and creates an electron transport **ET** (further than Q_A^-) that leads ultimately to CO_2 fixation.

Formulae relating the specific (per reaction center RC) and phenomenological energy fluxes (per excited cross section CS or leaf area), as well as the flux ratios or yields, with the experimental values provided from the JIP-test, have been derived on the basis of the energy flux theory (Strasser et al. 2000), as explained below:

The key expression of the JIP-test is $\mathbf{TR_0/RC}$, the specific trapping flux at time zero. At any time $\mathbf{TR/RC}$ expresses the rate by which an exciton is trapped by the RC resulting in the reduction of $\mathbf{Q_A}$ to $\mathbf{Q_A^-}$. The maximal value of this rate is given by $\mathbf{TR_0/RC}$, because at time zero all RCs are open. If the reoxidation of $\mathbf{Q_A^-}$ was blocked, as happens in DCMU-treated samples, $\mathbf{TR_0/RC}$ would be given by the normalization of the initial slope of the fluorescence induction curve (measured between 50 and 300μs) on the maximal variable fluorescence $\mathbf{F_V = F_M - F_0}$. This normalized value is denoted as $\mathbf{M_{0,DCMU}}$. However, since $\mathbf{Q_A^-}$ reoxidation is not blocked in vivo, the normalized value of the initial slope, $\mathbf{M_0}$, expresses the net rate of the RCs' closure, where trapping increases the number of closed centers and electron transport decreases it:

$$\mathbf{M_0 = TR_0/RC - ET_0/RC} \qquad \text{(eq. 51)}$$

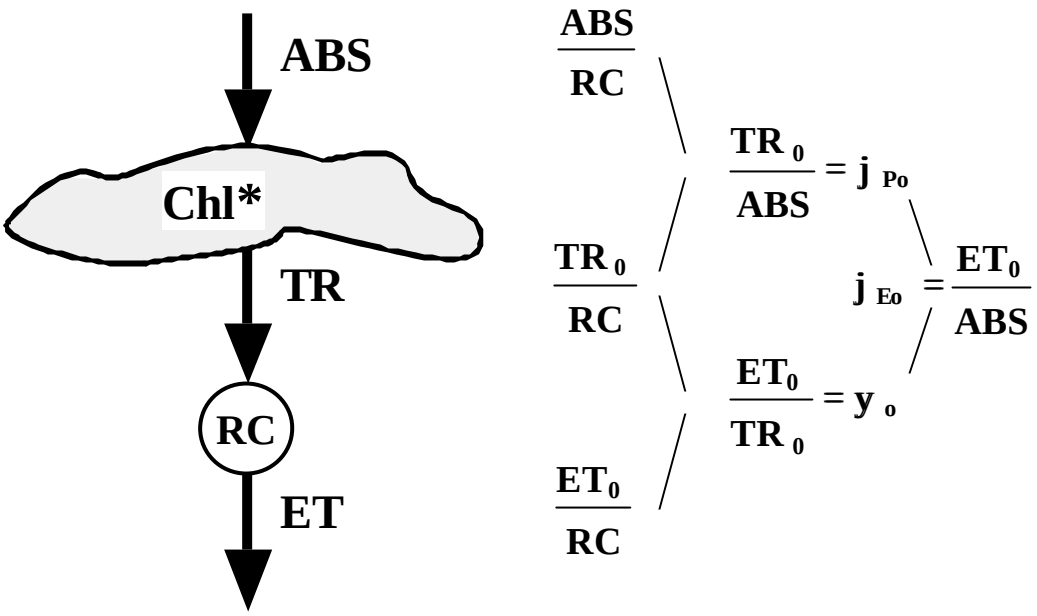

Fig. 5. A highly simplified scheme for the energy cascade from PSII light absorption to electron transport. (Based on a scheme by Strasser and Strasser 1995). For details see text.

A thorough investigation carried out in our laboratory (Strasser and Strasser 1995) revealed that the O-J phase, normalized between 0 and 1, coincides with the **V=f(t)** in DCMU-treated samples. Hence, $\mathbf{M_{0,DCMU}}$ can be simulated by the amplification of the in vivo measured $\mathbf{M_0}$ by a factor reciprocal to $\mathbf{V_J}$ or, equivalently, by the initial slope of **W=f(t)**, where

$$\mathbf{W \equiv V/V_J = (F-F_0)/(F_J - F_0)} \qquad \text{(eq. 52)}$$

Therefore, the maximal specific trapping flux is written as:

$$\mathbf{TR_0/RC = M_{0,DCMU} = M_0/V_J = (dW/dt)_0} \qquad \text{(eq. 53)}$$

Eqs. 51 and 53, give the maximal specific flux for electron transport further than $\mathbf{Q_A^-}$:

$$\mathbf{ET_0/RC = TR_0/RC - M_0 = (TR_0/RC) \cdot (1-V_J)} \qquad \text{(eq. 54)}$$

Hence, the probability that a trapped exciton moves an electron into the electron transport chain further than $\mathbf{Q_A^-}$ is given as:

$$\mathbf{\psi_0 \equiv ET_0/TR_0 = 1 - V_J} \qquad \text{(eq. 55)}$$

Since the maximum quantum yield of primary photochemistry is

$$\mathbf{\varphi_{Po} \equiv TR_0/ABS = 1 - (F_0 / F_M)} \qquad \text{(eq. 56)}$$

we get for the maximum yield of electron transport

$$\mathbf{\varphi_{Eo} \equiv ET_0/ABS = (TR_0/ABS) \cdot (ET_0/TR_0) = \varphi_{Po} \cdot \psi_0 = [1 - (F_0/F_M)] \cdot (1-V_J)} \qquad \text{(eq. 57)}$$

Combining eqs. 53 and 56 gives a measure for the average absorption per reaction center (**ABS/RC**) and, concomitantly, of the apparent antenna size, i.e. of the amount of absorbing chlorophylls per fully active (Q_A-reducing) reaction center:

$$\mathbf{ABS/RC = (TR_0/RC) / (TR_0/ABS) = (TR_0/RC)/ \varphi_{Po} = (M_0 / V_J)/[1 - (F_0 / F_M)]} \qquad \text{(eq. 58)}$$

The link between phenomenological and specific fluxes is the RCs' concentration (or density) per excited cross section of samples, **RC/CS**, which is given as:

$$\mathbf{RC/CS = (ABS/CS)/(ABS/RC)} \qquad \text{(eq. 59)}$$

Once **ABS/CS** is experimentally accessed, **RC/CS** is calculated and the set of phenomenological fluxes is:

$$\mathbf{ABS/CS = as\ measured} \qquad \text{(eq. 60)}$$

$$\mathbf{TR_0/CS = (TR_0/RC)\ (RC/CS)} \qquad \text{(eq. 61)}$$

$$\mathbf{ET_0/CS = (ET_0/RC)\ (RC/CS)} \qquad \text{(eq. 62)}$$

The value of **ABS/CS** is directly determined experimentally, hence being a measure of **Chl/CS**, in which case it is denoted as $\mathbf{ABS/CS_{Chl}}$. If this is not possible (like in field experiments), it can be approximated as:

$$\mathbf{ABS/CS_0 = F_0} \quad \text{or} \quad \mathbf{ABS/CS_M = F_M} \qquad \text{(eq. 60′)}$$

The criterion for the choice (subscripts "0" and "M" are used to make the distinction) is which of the yields $\mathbf{\varphi_{F_0}}$ or $\mathbf{\varphi_{F_M}}$ is unaffected by conformational differences of the samples or states to be compared. Concomitantly,

$$\mathbf{TR_0/CS_0 = [1 - (F_0 / F_M)] \cdot F_0} \quad \text{or} \quad \mathbf{TR_0/CS_M = [1 - (F_0 / F_M)] \cdot F_M} \qquad \text{(eq. 61′)}$$

$$\mathbf{ET_0/CS_0 = [1 - (F_0 / F_M)] \cdot (1-V_J) \cdot F_0} \quad \text{or} \quad \mathbf{ET_0/CS_M = [1 - (F_0 / F_M)] \cdot (1-V_J) \cdot F_M} \qquad \text{(eq. 62′)}$$

2. Non-Q_A-reducing reaction centers - Silent reaction centers functioning as heat sinks

Applying the JIP-test for studies on the behavior of PSII when photosynthetic organisms were exposed for a short time to light or heat stress, we witnessed, in most of the cases, that a pronounced decrease of $\mathbf{\varphi_{Po} = TR_0/ABS}$, measured as $\mathbf{F_V/F_M}$, and a stability of **TR_0/RC**, while no absorption

changes were detected (by reflectance measurements). We proposed (e.g. Tsimilli-Michael et al. 1998; Strasser and Tsimilli-Michael 1998; for a review see Strasser et al. 2000) that this apparent controversy is due to the transformation of some RCs to "heat sinks", i.e. to RCs that act as efficient exciton traps but dissipate all their excitation energy, as shown in model c (Fig. 2). The proposition for this kind of photochemically inactive RCs came originally from Cleland et al. (1986) and was integrated in Krause's work on photoinhibition (see e.g. Krause 1988; Krause et al. 1990), as a possible protective mechanism. We here propose the term "silent RCs", which we consider as more suitable than the terms previously used: these RCs can neither reduce Q_A nor back transfer their excitation energy to the antenna and so they do not contribute to the variable fluorescence, their fluorescence yield remaining constantly low and equal to that of open RCs; moreover, they are quickly re-activated as soon as the stress that provoked their transformation ceases.

While $\mathbf{F_V/F_M}$ refers to the whole sample and thus is an average value, $\mathbf{TR_0/ABS_{total}}$, the trapping flux $\mathbf{TR_0/RC}$ should read as $\mathbf{TR_0/RC_{active}}$ because it is calculated only from the kinetics of the variable fluorescence and it thus refers only to those RCs (photochemically active) that can reduce Q_A. Hence, the concomitant increase of **ABS/RC** or, more correctly $\mathbf{ABS_{total}/RC_{active}}$, does not mean a structural increase of the antenna size of a biochemical complex, but an increase of the apparent or "economic" antenna size, i.e. of the total absorption divided by the active RCs. Utilizing the JIP-test parameters, it is easy to calculate (Strasser and Tsimilli-Michael 1998) which fraction of the RCs that were active in the unstressed state (control, subscript "c"), remain active after stress (no subscript) and, equivalently what is the fraction transformed to silent RCs (subscript "si"):

$$\frac{RC_{active}}{(RC_{active})_c} = \frac{(ABS/RC_{active})_c}{(ABS/RC_{active})} = \frac{(M_0/V_J)_c}{(M_0/V_J)} \frac{[1-(F_0/F_M)]}{[1-(F_0/F_M)_c]} \qquad \text{(eq. 63)}$$

$$\frac{RC_{si}}{(RC_{active})_c} = 1 - \frac{(M_0/V_J)_c}{(M_0/V_J)} \frac{[1-(F_0/F_M)]}{[1-(F_0/F_M)_c]} \qquad \text{(eq. 64)}$$

3. Performance indexes and driving forces

Recently (for a review see Strasser et al. 2000) the performance index on absorption basis, $\mathbf{PI_{ABS}}$, was introduced as:

$$PI_{ABS} = \frac{g_{RC}}{1-g_{RC}} \cdot \frac{j_{Po}}{1-j_{Po}} \cdot \frac{y_o}{1-y_o} \qquad \text{(eq. 65a)}$$

where $\mathbf{g_{RC} = Chl_{RC}/Chl_{total}}$ is the fraction of reaction center chlorophylls relatively to the total chlorophyll content. Since $\mathbf{Chl_{total} = Chl_{antenna} + Chl_{RC}}$, we get $\mathbf{g_{RC}/(1\text{-}g_{RC}) = Chl_{RC}/Chl_{antenna} = RC/ABS}$. Hence:

$$PI_{ABS} = \frac{RC}{ABS} \cdot \frac{j_{Po}}{1-j_{Po}} \cdot \frac{y_o}{1-y_o} \qquad \text{(eq. 65b)}$$

Multiplying by the flux **ABS/CS**, so that a factor for the chlorophyll concentration per leaf cross section is integrated, leads to the definition of the performance index on cross section basis, $\mathbf{PI_{CS}}$:

$$PI_{CS} = \frac{RC}{CS} \cdot \frac{j_{Po}}{1-j_{Po}} \cdot \frac{y_o}{1-y_o} = \frac{ABS}{CS} \cdot PI_{ABS} \qquad \text{(eq. 66)}$$

Substitution of the biophysical by the experimental parameters (see Table 2) results in:

$$PI_{ABS} = \frac{1-(F_0/F_M)}{M_0/V_J} \cdot \frac{F_M - F_0}{F_0} \cdot \frac{1-V_J}{V_J} \qquad \text{(eq. 65b′)}$$

$$PI_{CS} = \frac{ABS}{CS} \cdot \frac{1-(F_0/F_M)}{M_0/V_J} \cdot \frac{F_M - F_0}{F_0} \cdot \frac{1-V_J}{V_J} \qquad \text{(eq. 66′)}$$

As defined, the performance index is a product of expressions of the form $[p_i/(1-p_i)]$, where the p_i (i=1, 2, …, n) stand for probabilities or fractions. Such expressions are well-known in chemistry, with p_i representing e.g. the fraction of the reduced and $(1-p_i)$ the fraction of the oxidized form of a compound, in which case $\log[p_i/(1-p_i)]$ expresses the potential or driving force for the corresponding oxido-reduction reaction (Nernst's equation). Extrapolating this inference from chemistry, the **log(PI)** can be defined as the total driving force (**DF**) for photosynthesis of the observed system, created by summing the partial driving forces for each of the several energy bifurcations (at the onset of the fluorescence rise O-J-I-P):

$$DF_{ABS} = \log(PI_{ABS}) = \log\left(\frac{RC}{ABS}\right) + \log\left(\frac{j_{Po}}{1-j_{Po}}\right) + \log\left(\frac{y_o}{1-y_o}\right) \qquad \text{(eq. 67)}$$

$$DF_{CS} = \log(PI_{CS}) = \log\left(\frac{ABS}{CS}\right) + \log\left(\frac{RC}{ABS}\right) + \log\left(\frac{j_{Po}}{1-j_{Po}}\right) + \log\left(\frac{y_o}{1-y_o}\right) \qquad \text{(eq. 68)}$$

Introducing the notations $DF_{Chl} = \log[ABS/CS]$, $DF_{RC} = \log[RC/ABS]$, $DF_j = \log[j_{Po}/(1-j_{Po})]$ and $DF_y = \log[y_o/(1-y_o)]$ for the partial driving forces, we can write the above equations as

$$DF_{ABS} = DF_{RC} + DF_j + DF_y \qquad \text{(eq. 67′)}$$

$$DF_{CS} = DF_{Chl} + DF_{RC} + DF_j + DF_y \qquad \text{(eq. 68′)}$$

4. The complementary area and the turnover number

The total complementary area (from time 0 to t_{Fmax}) is directly calculated from the digitized fluorescence rise:

$$Area = \int_0^{t_{F\,max}} (F_M - F_t)\,dt \qquad \text{(eq. 69)}$$

In order to compare different samples, the Area must be normalized by F_V. The normalized expression, defined as $S_m = Area / (F_M - F_0)$, expresses a work-integral, i.e. it gives a measure of the energy needed to close all reaction centers. Subscript "m" refers to the multiple turnover for the RCs' closure. The more the electrons from Q_A^- are transferred into the electron transport chain **ET**, the longer the fluorescence signals remain lower than F_M and the bigger S_m becomes. The smallest possible normalized total area corresponds to the case when each Q_A is reduced only once, as in the presence of DCMU, and it can then be denoted as S_S indicating single turnover. Thereafter, the so-called turn-over number **N**, defined as

$$N = \frac{S_m\ (\text{without DCMU, multiple turn-over})}{S_S\ (\text{with DCMU, single turn-over})} \qquad \text{(eq. 70)}$$

expresses how many times Q_A has been reduced in the time span from 0 to $t_{F_{max}}$.

If we consider an exponential fluorescence rise for the single turn-over situation, then the normalized area S_S would be inversely proportional to the initial slope of the relative variable fluorescence, i.e. $S_S = (M_{0,DCMU})^{-1}$. However, as above analyzed (see eq. 53), the value of this slope can be calculated utilizing only data from the in vivo fluorescence transient as $M_{0,DCMU} = M_0/V_J$, without the requirement of additional measurements in the presence of DCMU.

Hence, under in vivo conditions, $S_S = (M_0/V_J)^{-1} = V_J/(dV/dt)_0$ and eq. 70 is written as:

$$N = S_m \cdot [(dV/dt)_0] / V_J \qquad \text{(eq. 71)}$$

5. The time t_{F_M} to reach F_M and the average fraction of open reaction centers

The time to reach the maximal fluorescence is accurately determined only if $\mathbf{F_M}$ appears as a clear peak in the fluorescence transient. The ratio $\mathbf{S_m/t_{F_M}}$ expresses the average redox state of $\mathbf{Q_A}$ in the time span from 0 to t_{F_M}, namely the average (subscript "**av**") fraction of open reaction centers during the time needed to complete their closure:

$$\mathbf{S_m / t_{F_M} = [\, Q_A / Q_{A\,(total)} \,]_{av} = [\, 1 - (Q_A^- / Q_{A\,(total)}) \,]_{av} = 1 - B_{av}} \qquad \text{(eq. 72)}$$

This expression gives a measure of the average electron transport activity.

Furthermore, using eq. 29, the average quantum yield for primary photochemistry is given as:

$$\mathbf{j_{P,av} = TR_{av}/ABS = j_{Po}\,(1 - B_{av}) = j_{Po}\,(S_m/t_{F_M})} \qquad \text{(eq. 73)}$$

6. Determination of the over-all grouping probability

The JIP-test provides also the means to calculate the overall grouping probability in living samples in vivo and in situ, while all previous efforts were dealing with DCMU-inhibited or low-temperature-blocked photosynthetic material where the fluorescence transient reflects pure photochemical events. The basis of the calculation by the JIP-test is that, as explained above, the O-J part of the fluorescence transient reflects single turn over events, coinciding, when expressed as **W=f(t),** with the **V=f(t)** in DCMU-inhibited samples. Any exponential curve, with the J-level as asymptote, would present separate units. As tested by numerical simulations, the exponential curve $\mathbf{W_E=f(t)}$ corresponding to all the other features of the sample, crosses the actual curve **W=f(t)** at about 300 μs. The difference of the actual sigmoidal from the constructed exponential depends on the degree of grouping. The overall grouping probability $\mathbf{p_G}$ is calculated as follows, based on the maximal difference $\mathbf{W_{E(t)}\text{-}W(t)}$, which appears at 100 μs, so that the highest sensitivity is achieved (for details see Stirbet et al. 1998; Strasser and Stirbet 2001):

$$\mathbf{p_G} = \frac{(W_{E,100ms} - W_{100ms})}{W_{100ms}\,(1 - W_{E,100ms} V_J) V_J} \frac{F_0}{(F_M - F_0)} \qquad \text{(eq. 74)}$$

where

$$\mathbf{W_{E,\,100ms} = 1 - (1 - W_{300ms})^{(100-50)/(300-50)} = 1 - (1 - W_{300ms})^{1/5}}$$

$$\mathbf{W_{100ms} = \frac{F_{100ms} - F_{50ms}}{F_{2ms} - F_{50ms}}} \quad \text{and} \quad \mathbf{W_{300ms} = \frac{F_{300ms} - F_{50ms}}{F_{2ms} - F_{50ms}}}$$

The formulae were tested for leaves from the same plant (pea plant), with and without DCMU, and the calculated values of the overall grouping probability were very close, 0.26 and 0.25 respectively (Stirbet et al.1988; Strasser and Stirbet 2001).

7. Non-Q_B-reducing reaction centers

The PSII units can show a heterogeneity concerning the Q_A-Q_B binding. Adaptation processes can also regulate this heterogeneity, altering the fraction of the non-Q_B-reducing RCs. The fluorescence transient and the relaxation kinetics in the dark (Strasser et al. 1992) can provide an estimation of this fraction by numerical simulations (Strasser and Stirbet 1998). However, an easier and faster test can be used (Strasser and Tsimilli-Michael 1988), which utilizes two subsequent fluorescence transients O-J-I-P: The fluorescence transient recorded after a dark period long enough to ensure the re-opening of all RCs (denoted here as 1st hit) is followed by the induction of a second transient (denoted as 2nd hit and labeled as O*-J*-I*-P*) (Strasser and Govindjee 1992a, 1992b; Strasser et al. 1995; Strasser et al. 2001). The dark interval between the two hits is short enough to allow only the reopening of the Q_B-reducing RCs (fast reopening RCs). The duration of the dark interval is chosen

for each organism by experimental investigation of the fluorescence decay and, once this choice is done, the test comprising of the two subsequent hits can rapidly screen many samples. The experimental data (see e.g. Fig. 8) show that closed RCs which do not open within about 500 ms have to be considered as non-Q_B-reducing RCs (slow-reopening RCs).

Obviously F_0* is the resultant of fluorescence emitted by the units with still closed RCs (the non-Q_B reducing RCs, their fraction labeled as B_0) and units with open RCs (the fast reopening RCs, their fraction equal to 1- B_0). Assuming that the true F_0/F_M (fluorescence of all open RCs/ fluorescence of all closed RCs), F_0* can be regarded as a point on the fluorescence transient of the 1st hit. Hence,

$$\mathbf{1 - B_0^*} = \frac{(\mathbf{F_M^* - F_0^*})/\mathbf{F_M^*}}{(\mathbf{F_M - F_0})/\mathbf{F_M}} = \frac{\mathbf{F_V^*/F_M^*}}{\mathbf{F_V/F_M}} \quad \Rightarrow$$

$$\mathbf{B_0^*} = \mathbf{1} - \frac{\mathbf{F_V^*/F_M^*}}{\mathbf{F_V/F_M}} \qquad \text{(eq. 75)}$$

As shown by comparison with the results from numerical simulations, $\mathbf{B_0}$ offers a good approximation for the estimation of the fraction of non-Q_B reducing RCs.

8. Summarizing the JIP-test

The translation by the JIP-test of original data from a fluorescence transient to biophysical parameters that quantify the PSII behavior is summarized in Table 2. Note that many of the JIP-test parameters depend on each other. The independent parameters can be classified in a group of four parameters (e.g. $\mathbf{F_0/F_M}$, $\mathbf{V_{100ms}}$, $\mathbf{M_0}$ and $\mathbf{V_J}$) providing information about single turn-over events that are reflected on the O-J phase, and a group of three parameters (e.g. $\mathbf{V_I}$, $\mathbf{S_m}$ and $\mathbf{t_{Fmax}}$) related with multiple turn-over events.

The JIP-test provides adequate information about the behavior (structure, conformation and function) of the photosynthetic apparatus being at any physiological state. It can as well be used to study point by point the changes of this behavior, as changes of the parameters discussed above, during the whole P-S state transition, as demonstrated in Fig. 6 (from Strasser et al. 2000). Two actinic illuminations are used, both provided by the light source of the PEA- fluorimeter set at 3% or 100% (18 and 600 W m^{-2} respectively). An O-J-I-P transient is induced in a dark-adapted leaf, i.e. $^{\mathbf{d}}\mathbf{F=f(t)}$ ("**d**" standing for dark), by illumination for 1 s with 600 W m^{-2}. The leaf is readapted to dark for 10 s and then exposed for 10 min to the illumination of 18 W m^{-2}. Every 10 s a fluorescence transient, $^{\mathbf{l}}\mathbf{F=f(t)}$ ("**l**" standing for light), is induced by a 1 s light pulse of 600 W m^{-2} . All transients are recorded to be further analyzed by the JIP-test (Strasser et al. 2000). In such an experiment $^{\mathbf{l}}\mathbf{F_0}$ is approximated by $^{\mathbf{d}}\mathbf{F_0}$, while the utilization of far red between the sequential transients permits the recording of the accurate values of $^{\mathbf{l}}\mathbf{F_0}$ as well. Hence, beside obtaining all the information for the calculation of the JIP-test parameters, the utilization of $^{\mathbf{d}}\mathbf{F_0}$, $^{\mathbf{d}}\mathbf{F_M}$ and $^{\mathbf{d}}\mathbf{F_P}$ (in the dark) and $^{\mathbf{l}}\mathbf{F_0}$, $^{\mathbf{l}}\mathbf{F_M}$ and $^{\mathbf{l}}\mathbf{F_s}$ (in the light) leads to the calculation of all quenching indexes, e.g. $\mathbf{q_N}$, $\mathbf{q_P}$ (or **qQ**) and **NPQ** with a high quality signal to noise ratio.

C. The K-Step: A probe of the PSII donor side

Under various stress conditions, such as heat stress (Guissé et al. 1995a, 1995b; Srivastava and Strasser 1995, 1996, 1997; Srivastava et al. 1995, 1997; Strasser B. 1997; Lazár and Ilík 1997; Lazár et al. 1997a) or drought stress (Guissé et al. 1995b), an early step was found to appear in the fluorescence rise at about 200 ìs and was labeled, following an alphabetic order (from the latest to the earliest), as the K-step. Under strong heat stress (44 to 48°C), the K-step was predominant,

Table 2. The JIP-test formulae using data extracted from the fast fluorescence transient O-J-I-P

extracted and technical fluorescence parameters		
F_0	=	F_{50ms} , fluorescence intensity at 50ms
F_{100ms}	=	fluorescence intensity at 100ms
F_{300ms}	=	fluorescence intensity at 300ms
F_J	=	fluorescence intensity at the J-step (at 2ms)
F_I	=	fluorescence intensity at the I-step (at 30ms)
F_M	=	maximal fluorescence intensity
t_{F_M}	=	time to reach F_M , in ms
V_J	=	$(F_{2ms} - F_0) / (F_M - F_0)$
Area	=	area between fluorescence curve and F_M
$(dV/dt)_0 = M_0$	=	$4 . (F_{300} - F_0) / (F_M - F_0)$
S_m	=	Area / $(F_M - F_0)$
B_{av}	=	$1 - (S_m / t_{Fmax})$
N	=	$S_m . M_0 . (1 / V_J)$ turn over number of Q_A
quantum efficiencies or flux ratios		
$j_{Po} = TR_0 / ABS$	=	$[1 - (F_0 / F_M)] = F_V / F_M$
$j_{Eo} = ET_0 / ABS$	=	$[1 - (F_0 / F_M)] . y_0$
$y_0 = ET_0 / TR_0$	=	$(1 - V_J)$
specific fluxes or specific activities		
ABS / RC	=	$M_0 . (1 / V_J) . (1 / j_{Po})$
TR_0 / RC	=	$M_0 . (1 / V_J)$
ET_0 / RC	=	$M_0 . (1 / V_J) . y_0$
DI_0 / RC	=	$(ABS / RC) - (TR_0 / RC)$
phenomenological fluxes or phenomenological activities		
ABS / CS	=	$ABS/CS_{Chl} = Chl/CS$ or $ABS/CS_0 = F_0$ or $ABS/CS_M = F_M$
TR_0 / CS	=	$j_{Po} . (ABS / CS)$
ET_0 / CS	=	$j_{Po} . y_0 . (ABS / CS)$
DI_0 / CS	=	$(ABS/CS) - (TR_0 / CS)$
density of reaction centres		
RC / CS	=	$j_{Po} . (V_J / M_0) . ABS/CS$
performance indexes		
PI_{ABS}	=	$(RC/ABS) . [j_{Po} / (1 - j_{Po})] . [y_0 / (1 - y_0)]$
PI_{CS}	=	$(RC/CS) . [j_{Po} / (1 - j_{Po})] . [y_0 / (1 - y_0)]$
driving forces		
DF_{ABS}	=	$\log (PI_{ABS})$
DF_{CS}	=	$\log (PI_{CS}) = \log (PI_{ABS}) + \log (ABS/CS)$
Overall grouping probability		
p_{2G}	=	$\frac{(W_{E,100ms} - W_{100ms})}{W_{100ms} (1 - W_{E,100ms} V_J) V_J} - \frac{F_0}{(F_M - F_0)}$
	where:	$W_t = (F_t - F_{50ms}) / (F_{2ms} - F_{50ms})$
	and	$W_{E,100ms} = 1 - (1 - W_{300ms})^{1/5}$

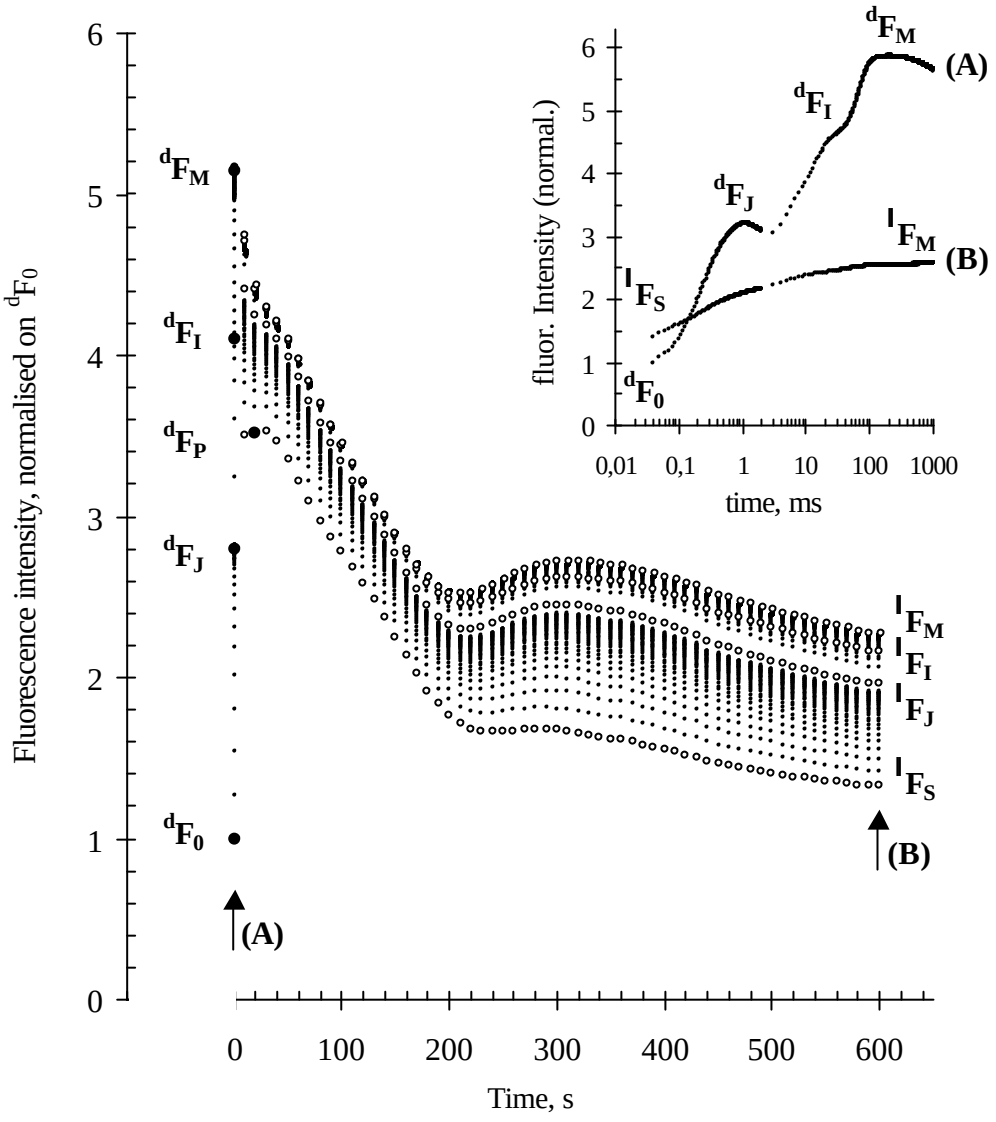

Fig. 6. Polyphasic fluorescence induction kinetics screening the P-S state-transition. Two actinic illuminations are used, both provided by the light source of the PEA-fluorimeter set at 3% or 100% (18 and 600 W m^{-2} respectively). An O-J-I-P transient is induced in a dark-adapted leaf, i.e. **^{d}F=f(t)** ("**d**" standing for dark), by illumination for 1 s with 600 W m^{-2}. The leaf is readapted to dark for 10 s and then exposed for 10 min to the illumination of 18 W m^{-2}. Every 10 s a fluorescence transient, **^{l}F=f(t)** ("**l**" standing for light), is induced by a 1 s light pulse of 600 W m^{-2}. Open circles show the fluorescence values at the distinct steps **^{l}F$_s$** (= **^{l}F$_P$**), **^{l}F$_J$** ,**^{l}F$_I$** and **^{l}F$_M$** , while the big closed circles the values at the steps of the transient exhibited by the dark-adapted sample. Indicatively, the fluorescence transients of the dark-adapted sample (A) and the sample adapted for 10 min to the illumination of 18 W m^{-2} (B) are depicted in the insert. All digitized transients are further analyzed by the JIP-test (Strasser et al. 2000).

followed by a pronounced dip and later by a slight increase to a highly suppressed P-step. However, further investigation showed that, under milder heat stress (40 to 44°C), fluorescence transients with distinct K- and J-steps, even separated by a dip, are exhibited; this excludes the possibility that the K-step is just a shifted J-step and shows that a regular O-J-I-P transient is transformed to an O-K-J-I-P one. Such a transient was also observed in algal culture of *Haematococcus lacustris* at certain phases of its life cycle, namely in the red flagellates and red spores, while green flagellates and green spores exhibited the K-step only after heat treatment (Srivastava et al. 1997). Moreover, the O-K-J-I-P transient is also exhibited by different higher plants growing naturally in ecosystems with dry and hot environment, like leaves of *Cycus revoluta* and *Permelia sp*., as well as fruits of *Juniperus sp*. (Srivastava et al. 1997). It was hence proposed that the process responsible for eliciting the K-step is a natural phenomenon in oxygenic plants, but the K-step is usually "hidden" in the O-J rise, due to the established balance between the several electron transport reactions responsible for the fluorescence rise; in the frame of this proposition the K-step appearance is considered as resulting from a deviation from the usually established balance (Srivastava et al. 1997).

It was suggested (Guissé et al. 1995a; Srivastava et al. 1995, 1997; Srivastava and Strasser 1996; Strasser B. 1997) that the K-step is related to the inactivation of the oxygen - evolving - complex (OEC) leading to an imbalance between the electron flow leaving the RC towards the acceptor side and the electron flow coming to the RC from the donor side, associated with the accumulation of a high fluorescence yield species (speculated to be the $Pheo^-$, see also section V.D) acting as precursor of Q_A^- . Evidences supporting this suggestion were provided by different experimental approaches: (a) In samples exposed to strong heat stress (see above), the addition of hydroxylamine in millimolar concentrations, known to act as an electron donor to PSII, restored to a big extent the regular shape of the fluorescence rise (Guissé et al. 1995a; Srivastava et al. 1995, 1997; Srivastava and Strasser 1996). (b) Addition of hydroxylamine in millimolar concentrations to non-heated samples, known also to extract manganese from the OEC beside restoring electron donation, resulted in the appearance of the K-step, however only under high light intensity (> 300 W m^{-2}) (Strasser B. 1997). (c) The 4-period oscillations of F_0 and F_J, related to the S-states of the OEC and revealed when the fluorescence induction is preceded by exposure to different numbers of single turn over flashes, disappear in heat treated samples similarly as in samples where the OEC was inactivated by hydroxylamine (Strasser B. 1997; Strasser and Strasser 1998). (d) In not-heated samples, the K-step appeared in the fluorescence rise when the OEC was brought, before the onset of illumination, to the S_3-state by pre-illumination with two single turn over flashes (Strasser B. 1997; Strasser and Strasser 1998); the S_3-state is known to have a much smaller rate constant for electron donation than the S_1-state which is the predominant one in dark-adapted samples ($S_3 \rightarrow S_4$ is about 15 times slower than $S_1 \rightarrow S_2$).

In accordance with the experimental results, simulations of the O-K-J-I-P (Lazár et al. 1997b) showed that the electron transfer from water to Y_Z is much slower than from Y_Z to $P680^+$, the rate limiting step being at the OEC. Breaking the OEC, the electron donation is facilitated, though limited due to the highly reduced availability of electrons, while addition of hydroxylamine (millimolar concentration) erases the limitation.

It appears that activation and inactivation of the OEC is a common regulation mechanism under in vivo conditions determined by the way how the manganese is bound in the complex. Information for the donor side both from the K-step and the period-4 oscillations of fluorescence signals at certain steps ($\mathbf{F_0}$, $\mathbf{F_K}$ and $\mathbf{F_J}$) of the fluorescence transient (Strasser B. 1997) can be utilized for further investigations of the behavior of PSII, as extensions of the JIP-test.

D. Numerical Simulations of the Polyphasic Fluorescence Rise

Simulations of experimental fluorescence transients are today so advanced that the fitting of the experimental data can be achieved with an accuracy ± 2% over the whole time span (20 ìs to 2 s,

i.e. 5 orders of magnitude). The simulations are based on the solution of systems of differential equations formulated on the basis of biochemical models of different complexity leve1s (Stirbet and Strasser 1995, 1996, 1998, 2001; Stirbet et al. 1998, 2001; Strasser and Stirbet 1998, 2001; Lazár et al. 1997b; Vredenberg 2000). Different models have incorporated different assumptions and/or combination of assumptions, i.e. grouping, oxidized plastoquinone quenching, dependence of the fluorescence yield on the donor side of PSII, i.e. on the S- states of the OEC.

Obviously, a precondition for the simulation and fitting of biochemical models with experimental data is the transformation of a fluorescence induction curve into a kinetic of the fraction of closed RCs. As pointed out in section C.2 the equivalences "low fluorescence yield units ⇔ open RCs" and "high fluorescence yield units ⇔ closed RCs" are identities, i.e. they express the definition of "open" and "closed" RC. On the other hand, the equivalences "open RCs ⇔ $\mathbf{Q_A}$" and "closed ⇔ $\mathbf{Q_A^-}$" are conceptual, based on the quencher theory of Duysens and Sweers (1963) and dogmatically accepted since then. However, during the last forty years, our knowledge regarding the composition and the structure of PS II has been completed with a lot of information, among which the role of Pheo as the primary electron acceptor (see e.g. Diner and Babcock 1996; Ke 2001). Hence, the equation $\mathbf{B = [Q_A^-]/[Q_A^{total}]}$ is brought under dispute and it becomes necessary to re-examine which are the biochemical species with high fluorescence yield.

In an effort to tackle this open question, a comparative study of simulations was carried out for three different possible approaches, all based on the same reaction scheme (shown in Fig. 7) with the electron transfer reactions at the acceptor side of PS II involving 12 biochemical species (see numbering in Fig. 7; **Pheo** is indicated as **Ph**) (Strasser and Stirbet 2001). For each one of these approaches that are formulated as follows, the fraction **B(t)** of "closed RCs", in the sense of high fluorescence yield species responsible for the fluorescence induction kinetics, is built up by distinct combinations of biochemical species:

(a) The widely accepted "classical" model (Duysens and Sweers 1963) in which $\mathbf{Q_A}$ acts as a quencher, i.e. "open RCs (low fluorescence yield) ⇔ $\mathbf{Q_A}$" and "closed RCs (high fluorescence yield) ⇔ $\mathbf{Q_A^-}$":

$$\mathbf{B = PhQ_A^-Q_B + Ph^-Q_A^-Q_B + PhQ_A^-Q_B^- + Ph^-Q_A^-Q_B^- + PhQ_A^-Q_B^{2-} + Ph^-Q_A^-Q_B^-}$$

(b) An extended version of the "classical model", proposed by Vrederberg (2000), according to which the species with only the primary quinone acceptor reduced ($\mathbf{Q_A^-}$) have half contribution to the building of **B(t)** compared to those with both primary acceptors reduced ($\mathbf{Ph^-}$ and $\mathbf{Q_A^-}$):

$$\mathbf{B=(1/2)(PhQ_A^-Q_B + PhQ_A^-Q_B^- + PhQ_A^-Q_B^{2-}) + Ph^-Q_A^-Q_B + Ph^-Q_A^-Q_B^- + Ph^-Q_A^-Q_B^{2-}}$$

(c) A model according to which only $\mathbf{Ph^-}$ is responsible for the fluorescence rise, i.e. **B(t)** is built up by all the species with reduced $\mathbf{Ph^-}$ (Strasser and Stirbet 2001):

$$\mathbf{B = Ph^-Q_AQ_B + Ph^-Q_A^-Q_B + Ph^-Q_AQ_B^- + Ph^-Q_A^-Q_B^- + Ph^-Q_AQ_B^{2-} + Ph^-Q_A^-Q_B^{2-}}$$

The simulations for all these three models, where grouping was also taken into account, let to fittings equally satisfactory (accuracy ± 2% over the whole time span 20 ìs to 2 s). Hence, the question about the best of the three models remains open for the moment. However, models (a) and (b) require an explanation why Q_A^- would result in high fluorescence yie1d since the RC still acts as a trap and **Pheo** can still be reduced, while model (c) is based entire1y on dynamic photochemical quenching due to the utilization of the RC excitation energy for the reduction of the primary acceptor **Pheo**.

E. Simultaneous measurements of fluorescence transients and P700 oxidation

Parallel to the primary charge separation $P680^+Pheo^-$ occurring after an exciton is transferred to the chlorophyll of the RC of PSII (P680→P680*), a similar sequence of events takes place in PSI: light

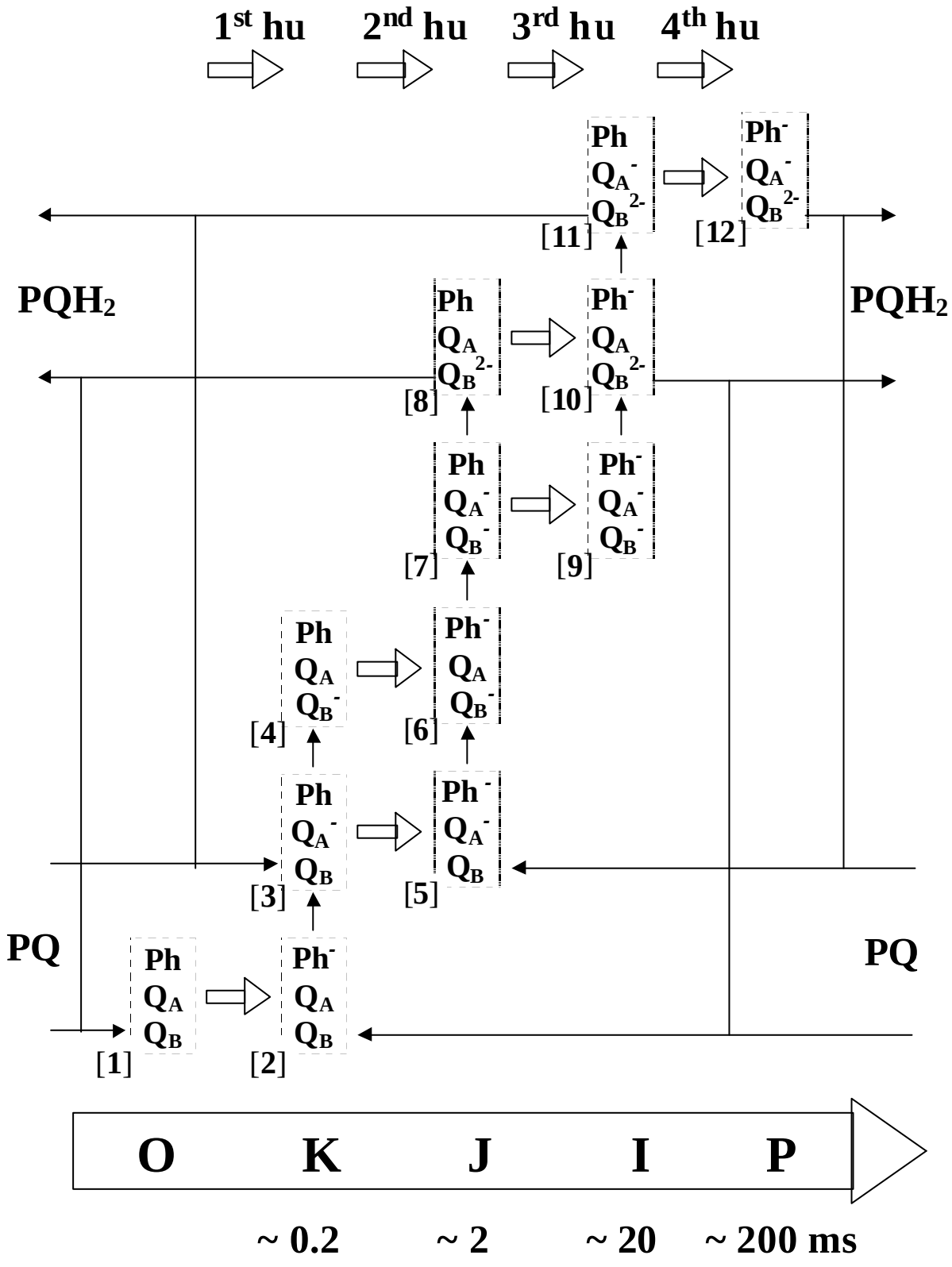

Fig. 7. The reaction scheme of the electron transfer reactions at the acceptor side of PS II reaction centre. Four light quanta are necessary for the complete reduction of the electron carriers (PhQ_AQ_B). The K-J-I-P phases of the fluorescence transient are correlated, depending on the model (see text), with the 12 distinct biochemical species (see numbering) formed during the accumulation of electrons in the three electron carriers (From Strasser and Stirbet 2001).

is absorbed by the PSI antenna, excitons are transferred to the chlorophyll of the reaction center of PSI (P700→P700*), and primary charge separation follows leading to $P700^+Ao$, where Ao is a bound chlorophyll monomer (like Pheo being a bound pheophytin molecule) (for details, see Ke 2001). In order to understand the interactions and the regulation of the two systems, it is necessary to measure simultaneous changes in the two systems. A large number of studies have dealt with the stoichiometry of PSI and PSII, using Chl *a* fluorescence as a monitor of Q_A reduction and thus of PSII activity, and absorption changes at 820 nm as a monitor of P700 oxidation (since Kok and Hoch 1961) and, hence, of PSI activity. An early attempt to measure, at 77 K, P700 absorption and Chl *a* fluorescence simultaneously was made by Strasser and Butler (1976) who studied "spill over" of excitation energy from PSII to PSI. Schreiber et al (1988) introduced parallel measurements for quantum yields of PSII (Chl *a* fluorescence) and PSI (absorbance change at 830 nm) in leaves by a modulated instrument. This method for simultaneous measurements of PSI and PSII was further improved by Havaux et al. (1991) and by Klughammer and Schreiber (1994, 1998), and recently exploited by Eichelmann and Laisk (2000) for the understanding of the cooperation between PSI and PSII in leaves.

Very recently, simultaneous measurements in pea plant leaves of the O-J-I-P kinetics of Chl *a* fluorescence (PSII) and the photo-oxidation of P700 (PSI, measured as light induced absorption changes at 820 nm) were conducted, with high time resolution (μs range), by using two shutter-less PEA fluorimeters, with the one modified to integrate a high frequency modulated measuring beam at 820 nm. Plotting the two kinetics, both induced by continuous red (650 nm) light of 3000 μmol m^{-2} s^{-1}, on a logarithmic time scale, revealed interesting correlations of the events at the two photosystems. In the presence of DCMU, which blocks the intersystem electron flow, an accumulation of $P700^+$, revealed as an absorbance increase at 820 nm (decrease of the photocurrent I) is observed throughout the whole time span from 20 μs to 2 s. On the other hand, the increasing Q_A^- concentration, reflected in the fluorescence rise, reaches its maximal value at about 2 ms and does not exhibit any further changes up to 2 s. In the non-treated leaves, the simultaneous measurements showed that from 20 μs to 20 ms, while the Q_A reduction to Q_A^- is giving rise to the O-I phase of the fluorescence transient, the kinetics of the P700 to $P700^+$ oxidation is identical to that in the presence of DCMU, which means that the two photosystems operate independently of each other, though there are not separated by any inhibitor. After 20 ms and until Q_A is fully reduced, i.e. during the I-P phase of the fluorescence transient, the two kinetics proceed almost in parallel, Q_A continuing to get reduced to Q_A^- but $P700^+$ getting re-reduced to P700 (for details see Strasser et al. 2001). These results show that only after 20 ms the plastoquinone pool, which is reduced by the PSII activity, starts to donate electrons to PSI.

A more detailed investigation was carried out by using two light pulses (red light - 650 nm of 3000 μmol m^{-2} s^{-1}) of 1 s duration, as illustrated in Fig. 8. The first pulse was given on a dark-adapted leaf, and the second one after different dark intervals (from 100 ms to minutes) following the first pulse. With this investigation (for details see Strasser et al. 2001) it was shown that the availability of intersystem electrons affects both the initial fluorescence, which offers a measure of the fraction $\mathbf{B_0}$ of closed RCs at time zero (note that the fluorescence kinetics are plotted as $\mathbf{V=f(t)}$, $\mathbf{V}$ the relative variable fluorescence) and the relative variable fluorescence at 2 ms ($\mathbf{V_J}$) which is considered as the end of the phase of single turnover events (section V.B), as well as the extent of the accumulation of $\mathbf{P700^+}$ (for details see Strasser et al. 2001).

F. Concluding Remarks and Future Perspectives

The analysis of the fluorescence transient O-J-I-P, as described above, has provided a lot of information. In our future perspectives we will proceed in further analysis of the transient, aiming advancements on two parallel axis, i.e. to tackle biophysical questions in order to achieve a better understanding of structure and function of the photosynthetic apparatus, and to extend the JIP-test for rapid screening of the vitality of plants.

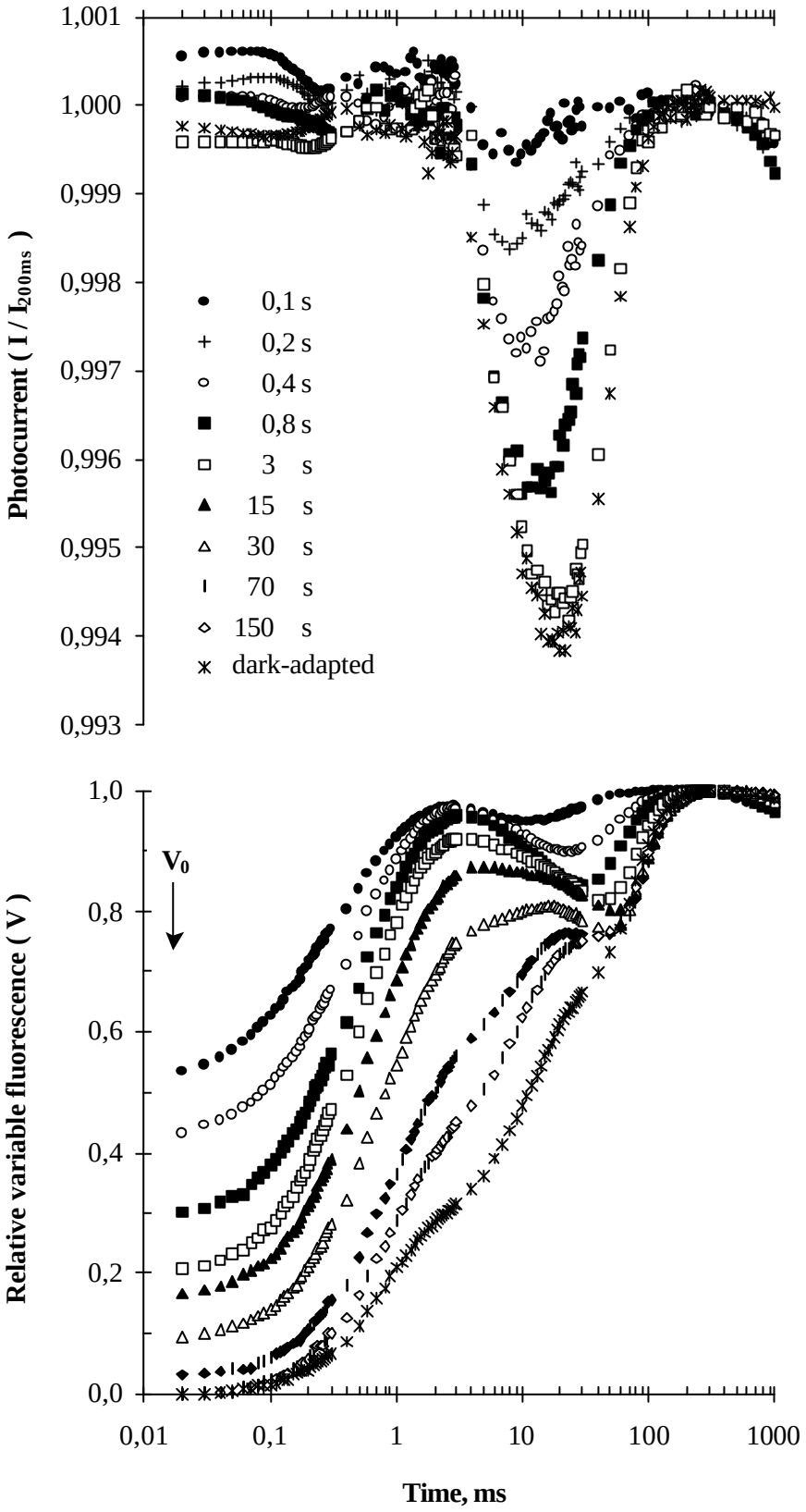

Fig. 8. Simultaneously measured induction kinetics of PS II, expressed by the O-J-I-P fluorescence transient (plotted as kinetics of the relative variable fluorescence **V**, bottom), and PS I, expressed by the photocurrent I at 820 nm (plotted as kinetics of $(I_t - I_{200ms})/ I_{200ms} = DI/I_{200ms}$, top), during a 1 s light pulse. The measurements were conducted in dark adapted samples (12 min dark, first pulse) and after various dark intervals (from 100 ms to minutes) following the first pulse (2^{nd} hits) as indicated in the figure.

Further investigations of simultaneously measured fluorescence transients and P700 oxidation will provide a better understanding of the function of both photosystems and the intersystem electron transport chain, as well as of the fluorescence signals, to be used both for routine vitality tests and for numerical simulations.

Ongoing simulations attempt to integrate delayed fluorescence, in order to provide recognition of specific charge recombination and back reactions from the acceptor to the donor side of PSII; an attempted reaction scheme (see Stirbet and Strasser 2001) aims to correlate the fast O-K-J-I-P prompt fluorescence trace with delayed fluorescence at the according steps and with potential dips between the steps both of the prompt and the delayed fluorescence traces, taking also into account the impact of the S-states of the water splitting system on the fluorescence rise (namely the period 4-oscillations). The question about the possible role of $Pheo^{-}$ remains open. More has also to be known about the possible influence of $P680^{+}$ on the fluorescence transient under in vivo conditions.

The JIP-test, as above analytically described, leads to a quantification of the PSII architecture and behavior. Numerical simulations verify that the formulae of the JIP-test, though derived with some theoretical compromises, give well-approximated parameters. These parameters describe the average architecture/behavior of the sample tested, but also provide means for the detection, characterization and quantification of the heterogeneity of the sample at certain levels, namely the non-Q_A and non-Q_B-reducing centers. All calculations and graphical presentations of the results can be directly conducted from the recorded fluorescence transients with the BIOLYSER program (created by R.M. Rodriguez, Bioenergetics Laboratory, University of Geneva, and freely available at http://www.unige.ch/sciences/biologie/bioen). The incorporation of information for the donor side heterogeneity provided from the K-step and the period-4 oscillations of fluorescence signals at certain steps ($\mathbf{F_0}$, $\mathbf{F_K}$ and $\mathbf{F_J}$) of the fluorescence transient in the JIP-test for routine screenings is in our future perspectives.

For the moment, only the numerical simulations utilize the whole of the O-J-I-P transient, which is very rich in information, while the JIP-test exploits very few data of the transient. Our aim is to incorporate in the routine vitality test further and detailed analysis of the digitized fluorescence kinetics, e.g. different normalizations, calculation of kinetics differences as well as of kinetics of time-derivatives. For example, when fluorescence transients exhibited by leaves of *Vigna unguiculata* that were grown under slight nitrogen-deficiency or no deficiency (control) were expressed as W=f(t) (i.e. normalized between 50 μs and 2 ms, see eq. 52) and the kinetics of $\Delta W_t = W_t - W_{t,control}$ was plotted, a pronounced peak (ΔK) appeared at about 200 μs, indicating a "disconnection" in the water splitting system (Schmitz et al. 2001).

The easiness to measure, under any conditions and in a short time, hundreds of fast fluorescence transient and the automatic data processing make the JIP-test a powerful tool for rapid screening of the vitality of plants, even more because field investigations can be conducted with high laboratory precision. The future extensions will further improve its diagnostic capabilities.

REFERENCES

Akoyunoglou G (1981) Assembly of functional components in chloroplast photosynthetic membranes. In: Akoyunoglou G (ed) Photosynthesis, Vol V, Chloroplast Development, pp 353--366. Balaban International Science Services, Philadelphia, PA

Briantais JM, Vernotte C, Krause GH and Weiss E (1986) Chlorophyll *a* fluorescence of higher plants: chloroplasts and leaves. In: Govindjee, Amesz J and Fork DC (eds) Light Emission by Plants and Bacteria, pp. 539--583. Academic Press, New York

Butler WL (1978) Energy distribution in the photochemical apparatus of photosynthesis. Ann Rev Plant Physiol 29: 345--378

Butler WL and Strasser RJ (1977a) Tripartite model for the photochemical apparatus of green plant photosynthesis. Proc Natl Acad Sci USA 74: 3382--3385

Butler WL and Strasser RJ (1977b) Effect of divalent cations on energy coupling between the light-harvesting chlorophyll *a/b* complex and PSII. In: Hall DA, Coombs J and Goodwin TW (eds) Photosynthesis '77, pp 11--20. The Biochemical Society, London

Clark AJ, Landolt W, Bucher J and Strasser RJ (1998) The response of *Fagus sylvatica* to elevated CO_2 and ozone probed by the JIP-test based on the chlorophyll fluorescence rise OJIP. In: De Kok LJ and Stulen I (eds) Responses of Plant Metabolism to Air Pollution and Global Change, pp 283--286. Backhuys Publishers, Leiden, The Netherlands

Clark AJ, Landolt W, Bucher J and Strasser RJ (2000) Beech (*Fagus sylvatica*) response to ozone exposure assessed with a chlorophyll *a* fluorescence performance index. Environmental Pollution 109: 501--507

Cleland RE, Melis A and Neale PJ (1986) Mechanism of photoinhibition: photochemical reaction center inactivation in system II of chloroplast. Photosynthesis Res 9: 79--88

Dau H (1994) Molecular mechanisms and quantitative models of variable photosystem II fluorescence. Photochem Photobiol 60: 1--23

Delosme R (1967) Etude de l'induction de fluorescence des algues vertes et des chloroplastes au debut d'une illumination intense. Biochim Biophys Acta 143: 108--128

Diner BA and Babcock GT (1996) Structure, dynamics, and energy conversion efficiency in photosystem II. In: Ort DR and Yokum CF (eds) Advances in Photosynthesis, Vol 4, Oxygenic Photosynthesis: The Light Reactions, pp 213--247. Kluwer Academic Publishers

Duysens LNM, Sweers HE (1963) Mechanism of two photochemical reactions in algae as studied by means of fluorescence. In: Japanese Society of Plant Physiologists (eds) Studies on Microalgae and Photosynthetic Bacteria, pp 353--372. University of Tokyo Press, Tokyo

Eichelmann H and Agu Laisk A (2000) Cooperation of photosystems II and I in leaves as analyzed by simultaneous measurements of chlorophyll fluorescence and transmittance at 800 nm. Plant Cell Physiol 41(2): 138--147

Genty B, Briantais J-M and Baker NR (1989) The relationship between the quantum yield of photosynthetic electron transport and quenching of chlorophyll fluorescence. Biochim Biophys Acta 990: 87-92

Govindjee (1995) Sixty-three years since Kautsky: chlorophyll *a* fluorescence. Aust J Plant Physiol 22: 131--160

Gruszecki WI, Kernen P, Krupa Z. and Strasser RJ (1994) Involvement of xanthophyll pigments in regulation of light-driven excitation quenching in light-harvesting complex of Photosystem II. Biochim Biophys Acta 1188: 235--242

Guissé B, Srivastava A and Strasser RJ (1995a) The polyphasic rise of the chlorophyll *a* fluorescence (O-K-J-I-P) in heat-stressed leaves. Archs Sci Genève 48: 147--160

Guissé B, Srivastava A. and Strasser RJ (1995b) Effects of high temperature and water stress on the polyphasic chlorophyll *a* fluorescence transient of potato leaves. In: Mathis P (ed) Photosynthesis: from Light to Biosphere, Vol. IV, pp. 913--916, Kluwer Academic Publishers, The Netherlands

Havaux M, Greppin H and Strasser RJ (1991) Functioning of photosystems I and II in pea leaves exposed to heat stress in the presence or absence of light: Analysis using in-vivo fluorescence, absorbance and photoacoustic measurements. Planta 186: 88--98

Joliot A and Joliot P (1964) Etude cinétique de la réaction photochimique libérant l'oxygène au cours de la photosynthèse. CR Acad Sci Paris 258: 4622--4625

Karapetyan NV, Shubin VV and Strasser RJ (1999) Energy exchange between the chlorophyll antennae of monomeric subunits within the photosystem I trimeric complex of the cyanobacterium *Spirulina*. Photosynthesis Res 61: 291--301

Kautsky H and Hirsch A (1931) Neue Versuche zur Kohlensäureassimilation. Naturwissenschaften 19: 964

Ke B (2001) Photosynthesis: Photobiochemistry and Photobiophysics. In: Govindjee (ed) Advances in Photosynthesis, Vol 10. Kluwer Academic Publishers, Dordrecht/ Boston/London

Kitajima M and Butler WL (1975) Quenching of chlorophyll fluorescence and primary photochemistry in chloroplasts by dibromothymoquinone. Biochim Biophys Acta 376: 105--115

Klughammer C and Schreiber U (1994) An improved method, using saturating light pulses, for the determination of photosystem I quantum yield via $P700^+$ absorbance changes at 830 nm. Planta 192: 261--268

Klughammer C and Schreiber U (1998) Measuring P700 absorbance changes in the near infrared spectral region with a dual wavelength pulse modulation system. In: Garab G (ed) Photosynthesis: Mechanisms and Effects, Vol V, pp 4357—4360. Kluwer Academic Publishers, The Netherlands

Kok B and Hoch G (1961) Spectral changes in photosynthesis. In: McElroy MD and Glass B (eds) Light and Life, pp 376--416, John Hopkins Press, Baltimore, MD

Krause GH (1988) Photoinhibition of photosynthesis. An evaluation of damaging and protective mechanisms. Physiol Plantarum 74: 566--574

Krause GH and Weiss E (1991) Chlorophyll fluorescence and photosynthesis: the basics. Annu Rev Plant Physiol Plant Mol Biol 42: 313--349

Krause GH, Somersalo S, Zumbusch E, Weyers B and Laasch H (1990) On the mechanism of photoinhibition in chloroplasts. Relationship between changes in fluorescence and activity of photosystem II. J Plant Physiol 136: 472--479

Krüger GHJ, Tsimilli-Michael M and Strasser RJ (1997) Light stress provokes plastic and elastic modifications in structure and function of photosystem II in camellia leaves. Physiol Plantarum 101: 265--277

Lavergne J and Trissl H-W (1995) Theory of fluorescence induction in photosystem II: Derivation of analytical expressions in a model including exciton-radical-pair equilibrium and restricted energy transfer between photosynthetic units. Biophys J 68: 2474--2492

Lazár D (1999) Chlorophyll *a* fluorescence induction. Biochim Biophys Acta 1412: 1--28

Lazár D and Ilík P (1997) High-temperature induced chlorophyll fluorescence changes in barley leaves. Comparison of the critical temperatures determined from fluorescence induction and from fluorescence temperature curves. Plant Sci 124: 159--164

Lazár D, Ilík P and Nauš J (1997a) An appearance of K-peak in fluorescence induction depends on the acclimation of barley leaves to higher temperatures. J Luminesc 72--74: 595--596

Lazár D, Nauš J, Matoušková M and Flašarová M (1997b) Mathematical modelling of changes in chlorophyll fluorescence inductiion caused by herbicides. Pestic Biochem Physiol 57: 200--210

Ley AC and Butler WL (1977) The distribution of excitation energy between photosystem I and photosystem II in *Porphyridium cruentum*. Photosynthetic Organelles--Special Issue of Plant and Cell Physiol, 22--46

Lombard F and Strasser RJ (1984) Evidence for spill over changes during state-1 to state-2 transition in green leaves. In: Sybesma C (ed) Advances in Photosynthesis Research III, pp 271--274. Martinus Nijhoff/Dr W Junk Publishers, The Hague

Munday and Govindjee (1969) Light induced changes in the fluorescence yield of chlorophyll *a in vivo*. III. The dip and the peak in the fluorescence transient of *Chlorella pyrenoidosa*. Biophys J 9: 1--21

Neubauer C and Schreiber U (1987) The polyphasic rise of chlorophyll fluorescence upon onset of strong continuous illumination: 1. Saturation characteristics and partial control by the photosystem II acceptor side. Z Naturforsch 42c: 1246--1254

Ouzounidou G, Moustakas M and Strasser RJ (1997) Sites of action of copper in the photosynthetic apparatus of maize leaves: Kinetic analysis of chlorophyll fluorescence, oxygen evolution, absorption changes and thermal dissipation as monitored by photoacoustic signals. Aust J Plant Physiol 24: 81--90

Paillotin G (1976) Movement of excitations in the photosynthetic domains of photosystem II. J theor Biol 58: 237--252

Papageorgiou G (1975) Chlorophyll fluorescence: an intrinsic probe of photosynthesis. In: Govindjee (ed) Bioenergetics of Photosynthesis, pp 319--371. Academic Press, New York

Schmitz P, Maldonado-Rodriguez R and Strasser RJ (2001) Evaluation of the nodulated status of *Vigna unguiculata* probed by the JIP-test based on the chlorophyll *a* fluorescence rise. In: Proceedings of the XII International Congress in Photosynthesis, Brisbane-Australia (in press)

Schreiber U, Klughammer C and Neubauer C (1988) Measuring P700 absorbance changes around 830 nm with a new type of pulse modulation system. Z Naturforsch 43c: 686-698

Sironval C, Strasser RJ and Brouers M (1981) Equivalence entre la théorie des flux et la théorie des relations entre proportions de pigments pour la description de la répartition de l' energie lumineuse absorbée par les membranes photoactives. Bull Acad Roy Belgique 67: 248--259

Sironval C, Strasser RJ and Brouers M (1984) The bioenergetic description of light energy migration in photoactive membranes; equivalence between the theory of the energy fluxes and the theory of the proportion of pigments forms to total pigments. In: Sironval C and Brouers M (eds) Protochlorophyllide Reduction and Greening, pp 307--316. Martinus Nijhoff/Dr W. Junk Publishers, The Hague/ Boston/Lancaster

Srivastava A and Strasser RJ (1995) How do land plants respond to stress temperature and stress light? Archs Sci Genève 48: 135--145

Srivastava A and Strasser RJ (1996) Stress and stress management of land plants during a regular day. J Plant Physiol 148: 445--455

Srivastava A and Strasser RJ (1997) Constructive and destructive actions of light on the photosynthetic apparatus. J Sci Ind Res 56: 133--148

Srivastava A, Greppin H and Strasser RJ (1995) Acclimation of land plants to diurnal changes in temperature and light. In: Mathis P (ed) Photosynthesis: from Light to Biosphere, Vol. IV, pp. 909--912. Kluwer Academic Publishers, The Netherlands

Srivastava A, Guisse B, Greppin H and Strasser RJ (1997) Regulation of antenna structure and electron transport in PSII of *Pisum sativum* under elevated temperature probed by the fast polyphasic chlorophyll *a* fluorescence transient OKJIP. Biochim Biophys Acta 1320: 95--106

Srivastava A, Strasser RJ and Govindjee (1999) Greening of peas: parallel measurements of 77 K emission spectra, OJIP chlorophyll *a* fluorescence transient, period four oscillation of the initial fluorescence level, delayed light emission, and P700*. Photosynthetica 3: 365--392

Stirbet AD and Strasser RJ (1995) Numerical simulation of the fluorescence induction in plants. Archs Sci Genève 48: 41--60

Stirbet AD and Strasser RJ (1996) Numerical simulation of the in vivo fluorescence in plants. Mathematics and Computers in Simulation 42: 245--253

Stirbet AD and Strasser RJ (1998) Fast recording of chlorophyll *a* fluorescence, modelling and numerical simulation as a tool to probe the interaction of living systems with our planet. In: Greppin H, Degli Agosti R and Penel C (eds) Coaction Between Living System and Planet, pp 101--115. University of Geneva

Stirbet AD and Strasser RJ (2001) The possible role of pheophytin in the fast fluorescence rise OKJIP. In: Proceedings of the XII International Congress in Photosynthesis, Brisbane-Australia (in press)

Stirbet AD, Govindjee, Strasser BJ and Strasser RJ (1998) Chlorophyll *a* fluorescence induction in higher plants: Modelling and numerical simulation. J theor Biol 193: 131--151

Stirbet AD, Srivastava A and Strasser RJ (1998) The energetic connectivity of PSII centres in higher plants probed *in vivo* by the fast fluorescence rise O-J-I-P and numerical simulations. In: Garab G (ed) Photosynthesis: Mechanisms and Effects, Vol V, pp. 4317--4320. Kluwer Academic Publishers, The Netherlands

Stirbet AD, Rosenau Ph, Ströder AC and Strasser RJ (2001) Parameter optimisation of fast chlorophyll fluorescence induction model. Mathematics and Computer in Simulations 56: 443--450

Strasser BJ (1997) Donor side capacity of photosystem II probed by chlorophyll *a* fluorescence transients. Photosynthesis Res 52: 147--155

Strasser BJ and Strasser RJ (1995) Measuring fast fluorescence transients to address environmental questions: The JIP-test. In: Mathis P (ed) Photosynthesis: from Light to Biosphere, Vol V, pp 977--980. Kluwer Academic Publishers, The Netherlands

Strasser BJ and Strasser RJ (1998) Oscillations of the chlorophyll *a* fluorescence related to the S-states of the oxygen evolving complex. In: Garab G (ed) Photosynthesis: Mechanisms and Effects, Vol V, pp. 4325--4328. Kluwer Academic Publishers, The Netherlands

Strasser RJ (1978) The grouping model of plant photosynthesis. In: Akoyunoglou G (ed) Chloroplast Development, pp 513--524. Elsevier/North Holland

Strasser RJ (1980) Bacteriorhodopsin and its position in the blue light syndrome. In: Senger H (ed) The Blue Light Syndrome, pp 25--29. Springer-Verlag, Berlin

Strasser RJ (1981) The grouping model of plant photosynthesis: heterogeneity of photosynthetic units in thylakoids. In: Akoyunoglou G (ed) Photosynthesis III. Structure and Molecular Organisation of the Photosynthetic Apparatus, pp 727--737. Balaban International Science Services, Philadelphia, Pa

Strasser RJ (1984) The dynamics of the photoreduction of protochlorophyll(ide) into chlorophyll(ide). In: Sironval C and Brouers M (eds) Protochlorophyllide Reduction and Greening, pp. 317--327. Martinus Nijhoff/Dr W Junk Publishers, The Hague/Boston/Lancaster

Strasser RJ (1985) Dissipative Strukturen als Thermodynamischer Regelkreis des Photosyntheseapparates. Ber Deutsche Bot Ges Bd 98: 53--72

Strasser RJ (1986) Mono- bi- tri- and polypartite models in photosynthesis. Photosynthesis Res 10: 255--276

Strasser RJ (1988) A concept for stress and its application in remote sensing. In: Lichtenthaler HK (ed) Applications of Chlorophyll Fluorescence, pp 333--337. Kluwer Academic Publishers

Strasser RJ and Butler WL (1976) Energy transfer in the photochemical apparatus of flashed bean leaves. Biochim Biophys Acta 449: 412-419

Strasser RJ and Butler WL (1977a) Energy transfer and distribution of excitation energy in the photosynthetic apparatus of spinach chloroplasts. Biochim Biophys Acta 460: 230--238

Strasser RJ and Butler WL (1977b) The yield of energy transfer and the spectral distribution of excitation energy in the photochemical apparatus of flashed bean leaves. Biochim Biophys Acta 462: 295--306

Strasser RJ and Butler WL (1977c) Fluorescence emission spectra of photosystem I, photosystem II and the light-harvesting chlorophyll *a*/*b* complex of higher plants. Biochim Biophys Acta 462: 307—313

Strasser RJ and Butler WL (1977d) Energy coupling in the photosynthetic apparatus during development. pp. In: Hall DA, Coombs J and Goodwin TW (eds) Photosynthesis '77, pp 527--535. The Biochemical Society, London

Strasser RJ and Butler WL (1980) Interactions of flavins with cytochrome c and oxygen in excited artificial systems. In: Senger H (ed) The Blue Light Syndrome, pp 205-211. Springer--Verlag, Berlin

Strasser RJ and Govindjee (1992a) The F_0 and the O-J-I-P fluorescence rise in higher plants and algae. In: Argyroudi-Akoyunoglou JH (ed) Regulation of Chloroplast Biogenesis, pp 423--426. Plenum Press, New York

Strasser RJ and Govindjee (1992b) On the O-J-I-P fluorescence transient in leaves and D1 mutants of *Chlamydomonas Reinhardtii*. In: Murata N (ed) Research in Photosynthesis, Vol. 4, pp 29--32. Kluwer Academic Publishers, Dordrecht

Strasser RJ and Greppin H (1981) Primary reactions of photochemistry in higher plants, In: Akoyunoglou G (ed) Photosynthesis III. Structure and Molecular Organisation of the Photosynthetic Apparatus, pp 717--726. Balaban International Science Services, Philadelphia, PA

Strasser RJ and Stirbet AD (1998) Heterogeneity of photosystem II probed by the numerically simulated chlorophyll *a* fluorescence rise (O-J-I-P). Mathematics and Computers in Simulation 48: 3--9

Strasser RJ and Stirbet AD (2001) Estimation of the energetic connectivity of PS II centres in plants using the fluorescence rise O-J-I-P. Fitting of experimental data to three different PS II models. Mathematics and Computers in Simulation 56: 451--461

Strasser RJ and Tsimilli-Michael M (1998) Activity and heterogeneity of PSII probed *in vivo* by the chlorophyll *a* fluorescence rise O-(K)-J-I-P. In: Garab G (ed) Photosynthesis: Mechanisms and Effects, Vol V, pp. 4321--4324. Kluwer Academic Publishers, The Netherlands

Strasser RJ and Tsimilli-Michael M (2001) Structure function relationship in the photosynthetic apparatus: a biophysical approach. In: Pardha Saradhi P (ed) Biophysical Processes in Living Systems, Chapter 16, pp 271 -- 303. Science Publishers, Inc. Enfield (NH), USA

Strasser RJ and Tsimilli-Michael M (2001) Stress in plants, from daily rhythm to global changes, detected and quantified by the JIP-Test. Chimie Nouvelle (SRC) (in press)

Strasser RJ, Schwarz B and Bucher JB (1987) Simultane Messung der Chlorophyll Fluoreszenz-Kinetik bei verschiedenen Wellenlängen als rasches Verfahren zur Frühdiagnose von Immissionsbelastungen an Waldbäumen: Ozoneinwirkungen auf Buchen und Pappeln. Eur J For Path 17 (3): 149--157

Strasser RJ, Schwarz B and Eggenberg P (1988) Fluorescence routine tests to describe the behaviour of a plant in its environment. In: Lichtenthaler HK (ed) Applications of Chlorophyll Fluorescence, pp 181--187. Kluwer Academic Publishers

Strasser RJ, Eggenberg P, Pfister K and Govindjee (1992) An equilibrium model for electron transfer in photosystem II acceptor complex: an application to *Chlamydomonas reinhardtii* cells of D1 mutants and those treated with formate. Archs Sci Genève 45: 207--224

Strasser RJ, Srivastava A and Govindjee (1995) Polyphasic chlorophyll *a* fluorescence transient in plants and cyanobacteria. Photochem Photobiol 61: 32--42

Strasser RJ, Tsimilli-Michael M and Greppin H (1997) How excitation energy distribution indicates the complexity of a developing and to the environment adapting photosynthetic apparatus. In: Greppin H, Penel C and Simon P (eds) Travelling Shot on Plant Development, pp 99--129. University of Geneva

Strasser RJ, Srivastava A and Tsimilli-Michael M (1999) Screening the vitality and photosynthetic activity of plants by the fluorescence transient. In: Behl RK, Punia MS and Lather BPS (eds) Crop Improvement for Food Security, pp. 72--115. SSARM, Hisar, India

Strasser RJ, Srivastava A and Tsimilli-Michael M (2000) The fluorescence transient as a tool to characterize and screen photosynthetic samples. In: Yunus M, Pathre U and Mohanty P (eds) Probing Photosynthesis: Mechanism, Regulation and Adaptation, Chapter 25, pp 443--480. Taylor and Francis, London, UK

Strasser RJ, Schansker G, Srivastava A and Govindjee (2001) Simultaneous measurement of photosystem I and photosystem II probed by modulated transmission at 820 nm and by chlorophyll *a* fluorescence in the sub ms to second time range. In: Proceedings of the XII International Congress in Photosynthesis, Brisbane-Australia (in press)

Trissl H-W and Lavergne J (1995) Fluorescence induction from photosystem II: analytical equations for the yields of photochemistry and fluorescence derived from analysis of a model including exciton--radical pair equilibrium and restricted energy transfer between photosynthetic units. Aust J Plant Physiol 22: 183--193

Tsala G and Strasser RJ (1984) Energy distribution changes during phosphorylation of the light-harvesting complex in thylakoids In: Sybesma C (ed) Advances in Photosynthesis Research III, pp 279--282. Martinus Nijhoff/Dr W Junk Publishers, The Hague

Tsimilli-Michael M and Strasser RJ (2001) Mycorrhization as a stress adaptation procedure. In: Gianinazzi S, Haselwandter K, Schüepp H and Barea JM (eds) Mycorrhiza Technology in Agriculture: from Genes to Bioproducts. Birkhauser Basel, (in press)

Tsimilli-Michael M and Strasser RJ (2001) Fingerprints of climate changes on the photosynthetic apparatus' behaviour, monitored by the JIP-test. In: Walther G-R, Burga CA and Edwards PJ (eds) "Fingerprints" of Climate Changes – Adapted Behaviour and Shifting Species Ranges, pp 229--247. Kluwer Academic/Plenum Publishers, New York and London

Tsimilli-Michael M, Krüger GHJ and Strasser RJ (1995) Suboptimality as driving force for adaptation: A study about the correlation of excitation light intensity and the dynamics of fluorescence emission in plants, In: Mathis P (ed) Photosynthesis: from Light to Biosphere, Vol V, pp 981--984. Kluwer Academic Publishers, The Netherlands

Tsimilli-Michael M, Krüger GHJ and Strasser RJ (1996) About the perpetual state changes in plants approaching harmony with their environment. Archs Sci Genève 49: 173--203

Tsimilli-Michael M, Pêcheux M and Strasser RJ (1998) Vitality and stress adaptation of the symbionts of coral reef and temperate foraminifers probed *in hospite* by the fluorescence kinetics O-J-I-P. Archs. Sci. Genève 51 (2): 1--36

Tsimilli-Michael M, Pêcheux M and Strasser RJ (1999) Light and heat stress adaptation of the symbionts of temperate and coral reef foraminifers probed *in hospite* by the chlorophyll *a* fluorescence kinetics O-J-I-P. Z Naturforsch 54C: 671--680

Tsimilli-Michael M, Eggenberg P, Biro B, Köves-Pechy K, Vörös I and Strasser RJ (2000) Synergistic and antagonistic effects of arbuscular mycorrhizal fungi and *Azospirillum* and *Rhizobium* nitrogen-fixers on the photosynthetic activity of alfalfa, probed by the chlorophyll *a* polyphasic fluorescence transient O-J-I-P. Applied Soil Ecology 15: 169--182

Van Rensburg L, Krüger GHJ, Eggenberg P and Strasser RJ (1996) Can screening criteria for drought resistance in *Nicotiana tabacum L.* be derived from the polyphasic rise of the chlorophyll *a* fluorescence transient (OJIP)? S Afr J Bot 62 (6): 337--341

Vredenberg WJ (2000) A 3-state model for energy trapping and fluorescence in PSII incorporating radical pair recombination. Biophys J 79: 26--38